NASA/TM–2016-219168

Experimental Photogrammetric Techniques Used on Five Full-Scale Aircraft Crash Tests

Justin D. Littell
Langley Research Center, Hampton, Virginia

March 2016

NASA STI Program . . . in Profile

Since its founding, NASA has been dedicated to the advancement of aeronautics and space science. The NASA scientific and technical information (STI) program plays a key part in helping NASA maintain this important role.

The NASA STI program operates under the auspices of the Agency Chief Information Officer. It collects, organizes, provides for archiving, and disseminates NASA's STI. The NASA STI program provides access to the NTRS Registered and its public interface, the NASA Technical Reports Server, thus providing one of the largest collections of aeronautical and space science STI in the world. Results are published in both non-NASA channels and by NASA in the NASA STI Report Series, which includes the following report types:

- TECHNICAL PUBLICATION. Reports of completed research or a major significant phase of research that present the results of NASA Programs and include extensive data or theoretical analysis. Includes compilations of significant scientific and technical data and information deemed to be of continuing reference value. NASA counter-part of peer-reviewed formal professional papers but has less stringent limitations on manuscript length and extent of graphic presentations.

- TECHNICAL MEMORANDUM. Scientific and technical findings that are preliminary or of specialized interest, e.g., quick release reports, working papers, and bibliographies that contain minimal annotation. Does not contain extensive analysis.

- CONTRACTOR REPORT. Scientific and technical findings by NASA-sponsored contractors and grantees.

- CONFERENCE PUBLICATION. Collected papers from scientific and technical conferences, symposia, seminars, or other meetings sponsored or co-sponsored by NASA.

- SPECIAL PUBLICATION. Scientific, technical, or historical information from NASA programs, projects, and missions, often concerned with subjects having substantial public interest.

- TECHNICAL TRANSLATION. English-language translations of foreign scientific and technical material pertinent to NASA's mission.

Specialized services also include organizing and publishing research results, distributing specialized research announcements and feeds, providing information desk and personal search support, and enabling data exchange services.

For more information about the NASA STI program, see the following:

- Access the NASA STI program home page at http://www.sti.nasa.gov

- E-mail your question to help@sti.nasa.gov

- Phone the NASA STI Information Desk at 757-864-9658

- Write to:
  NASA STI Information Desk
  Mail Stop 148
  NASA Langley Research Center
  Hampton, VA 23681-2199

NASA/TM–2016-219168

Experimental Photogrammetric Techniques Used on Five Full-Scale Aircraft Crash Tests

Justin D. Littell
Langley Research Center, Hampton, Virginia

National Aeronautics and
Space Administration

Langley Research Center
Hampton, Virginia 23681-2199

March 2016

Available from:

NASA Center for AeroSpace Information
7115 Standard Drive
Hanover, MD 21076-1320
443-757-5802

Introduction

NASA Langley Research Center's (LaRC) Landing and Impact Research Facility (LandIR) has a long and rich history of full-scale aircraft crash testing. The facility, originally built in 1965 to train the Apollo astronauts for the moon landings, was converted into a full-scale crash test facility in 1972. It is a 240-ft. high, 400-ft. long steel A-frame gantry structure which uses a cabling system to pendulum swing test articles achieving various combinations of free flight and crash velocities [1]. Full-scale aircraft crash testing has been ongoing for 40+ years, with test articles ranging from small general aviation (GA) airplanes to large military transport helicopters. A partial history of testing up through the late 1990's is summarized in [2], with more recent tests summarized in references 3 through 7. Figure 1 shows the LandIR facility.

Figure 1 - LandIR facility

The use of video data acquisition in crash testing has always played an integral part in post-test failure analysis and crash reconstruction. The use of video data supplements the onboard sensor instrumentation suite which can include load, strain, acceleration and/or displacements of the aircraft structure, and it is only by the use of these two types of data together can a complete picture of each test be fully understood. The video data obtained can be categorized as either being used qualitatively or quantitatively. Ideally, video data would be fully quantitative such that definitive measurements can be obtained from examination of the recorded videos. However, often times the video data are qualitative in nature, showing generalized locations and event timing, but incapable of providing discrete numerical results. One example involves imaging an Anthropomorphic Test Device (ATD, a.k.a. crash test dummy) during an impact in order to track arm flail and/or head and chest rotation to determine whether strike onto an obstruction occurred without being able to compute the total magnitude of displacement.

Oftentimes, due to the range of impact velocities that are commonly associated with crash and/or dynamic impact testing, high-speed (>100 frames per second) camera systems are used. High-speed camera systems offer the ability to first record the impact sequence (ideally from multiple angles), and then review in slow motion in order to investigate the initiation and propagation of failure modes, which occur too fast to be captured using standard speed cameras or observable with just the naked eye.

High-speed camera and imaging systems at LandIR have historically consisted of analog film-based camera systems, recording on 16 mm. film at maximum rates of 400 Hz. for a maximum recording time of up to 20 sec., depending on the physical length of film being used. These cameras were either used as ground cameras filming a stationary view typically of the impact site, or tracking cameras, which follow the test article through the entire test sequence. In a small subset of tests, the cameras were placed onboard a test article and focused on a specific experiment. There were many negative aspects to using these film-based high-speed cameras: they were heavy, contained many moving mechanical parts, and they needed large amounts of power and lighting to work effectively.

In order to obtain useful data from the crash tests, points of interest need to be identified in advance. Common ways are to highlight frames, stringers and longitudinal structural members of the aircraft to track deformation. Other times, discrete targets are placed at structural junctions, ATD limbs or other areas of interest to gather specific results at those locations. Figure 2 shows one example on a GA test conducted in 1977 where the test article was painted a light yellow, over which the stiffeners, frame sections and rivet line locations were painted with black lines. There are yellow and black (commonly called "bowtie") stickers applied at the CG on the door and near the bottom of the firewall locations. No other types of tracking targets are visible.

Figure 2 - Historical painted patterns for use in tracking

Figure 2 also shows a white grid background, along with a grid pattern painted into the impact surface. The grid pattern in the background is located on a movable backboard (still in use) that can be placed behind the impact location specified by the test conditions. Both of these items were used to provide a reference

for and establish scaling factors in the analysis data, along with providing vertical, horizontal and lateral lines for orientation analysis from the video footage.

Since the mid-2000s, digital high-speed cameras have become robust enough to be consistantly used in crash and impact testing. Digital high-speed cameras are much better suited for use during impact tests, much more so than their analog counterparts: they contain no moving parts, contain no film and the memory can be reused, which offer ways to check focusing, lighting and other parameters through external monitors. They can also be triggered and re-triggered many times before the actual event to identify and mitigate potential problems prior to the actual test. Digital high-speed cameras have since replaced their film counterparts for the ground, tracking and onboard camera regimes. Because of their robustness, many of the high-speed cameras now are used exclusively in conjunction with the acquistion of photogrammetric data obtained from impact tests. The criticality of photogrammetric results has only recently been recognized as another piece of important data needed from each test.

Photogrammetric background

Photogrammetry can most simply be thought of as the acquisition of data from pictures, and has been in existence in one form or another since invention of the camera itself. In its simplest form, the approximate size or location of an object under investigation can be determined by using context clues from its surroundings. This type of qualitative analysis has existed since the advent of the picture itself. The recognition of photogrammetric data as a viable engineering tool became apparent in the early 1980s with the advent of digital cameras and the first personal computing systems. These products enabled the photogrammetric analysis to be semi or fully automated using computer algorithms, and moved the process into the semi-to-fully quantitative regime. And when applied to a sequence of images obtained through video capture, fully automated motion analysis can be achieved. A subset of photogrammetry, called full field digital image correlation (DIC), takes the processing even further and allows for the quantitative deformation field to be resolved on the entire object under investigation, providing data at many locations on the object. In this technique, hundreds or even thousands of data points are obtained on a single object and displayed as a fringe overlay, much like what is seen on finite element results.

In the more recent decade, the falling cost and higher quality of digital (and especially high-speed) cameras and the increased computing power available for use in processing the image data has brought these techniques from conceptual-development-only tools into the mainstream and are now widely used in industry. Photogrammetric techniques, and especially digital image correlation, are quickly being recognized as viable alternatives for deformation analysis, and can take the place of conventional instruments such as strain gages and linear displacement potentiometers in many applications which require precise position and deformation measurements. Numerous commercial companies have recognized this opportunity and have developed software and hardware packages which are turnkey in nature. These systems have become so robust that in some instances, an article under evaluation can be prepared, tested, imaged, and results processed in one afternoon, making a fast and simple measurement.

Large scale structures, and especially large scale structures undergoing dynamic loading, are prime examples of pushing the envelope in the application of these photogrammetric techniques. When evaluating large scale structures undergoing deformation, in some cases applying hundreds of strain gages to the surface is impractical, and in many cases impossible. A photogrammetric solution offers an ideal alternative due to the simplicity of the preparation process and the ease of pattern application. In many cases, it is the *only* way to obtain deformation data.

High-speed imaging for use in photogrammetric techniques matured during NASA's Return to Flight efforts [8], in the early 2000s, with software development proceeding rapidly to accommodate images acquired from digital high-speed cameras. And at large scales, photogrammetric techniques have been used to examine the shell buckling knock down factor on a large tubular rocket casing [9], evaluate deformation on a Hypersonic Inflatable Aero Decelerator (HIAD) during wind tunnel tests [10-11], and even served to provide deformation data from problems arising from the Space Shuttle External Tank Stringer Crack issue from STS-133 [12]. There are numerous other examples available which can be found through simple internet searches.

All of the cited examples above are presented to show a photogrammetric technique being used on either large structures or challenging environments, or both. These types of tests contain inherent difficulties, while at the same time they push the envelope in photogrammetric data acquisition techniques**.** In many of these instances, the difficulty lies in the logistics of merely obtaining and storing the image data from the cameras due to constraints in available space, power requirements, environmental factors, accessibility, or a combination thereof. If these logistical challenges can be overcome, ensuring successful data acquisition on the first try, and in many instances from a single test, requires that knowledge about potential weaknesses in setup, triggering, and/or data storage with steps in place to mitigate such problems if (or more appropriately, *when*) they inevitably arise. Finally, if successful acquisition of image data is achieved, many non-standard test results require that custom calibration and/or data processing techniques be developed before data can even be reported. It is usually by overcoming a combination of the above mentioned issues that mission success is ensured.

More recently, newer imaging systems and hardware are starting to be developed which do not use conventional pattern recognition or dot tracking techniques as with the traditional photogrammetric systems. In one example which will be evaluated in this report, a particular hardware sensor projects its own tracking pattern on a test subject, and recognizes the pattern deformation resulting from the interference of a subject in its view, resulting in a full three-dimensional solution.

The results and discussion in this report will focus on some of the various aspects of photogrammetric data acquisition, rationale for use, and results obtained in use at LandIR, and represents the state-of-the-art at the time of writing. The photogrammetric data primarily consists of discrete target tracking for use in determining impact conditions and post impact test article behavior from both high-speed and regular speed, high-definition cameras. Full field techniques include the use of digital image correlation for both 2-dimensional (2-D) and 3-dimensional (3-D) deformation tracking and the use of a markerless tracking sensor. Other example results are presented using the onboard high-speed cameras for tracking of ATD and structural response. These techniques were used on a small subset of the many tests conducted at the LandIR facility between 2013 and 2015, which were from the TRACT and ELTSAR test series. It must be noted that as new software and hardware becomes available, it will also be evaluated for potential use on future test articles, when applicable.

TRACT Test Series

The TRACT test series was a highly collaborative effort between NASA LaRC, Naval Air Systems Command (NAVAIR), FAA Civil Aeromedical Institute (CAMI), U.S. Army Aeromedical Research Laboratory (USAARL), U.S. Army Cargo Helicopter Project Management Office, and commercial companies. Each collaborator was investigating a variety of crashworthiness systems such as ATDs, restraint devices, and seats. One full year was needed to plan, identify experiments, collaborate, instrument

and crash each test article, with two crash tests conducted. The first, known as TRACT 1, was conducted on August 28, 2013 [5], and the second, known as TRACT 2, was on October 1, 2014 [6].

There were minor differences in the experimental suite between TRACT 1 and TRACT 2, and differences on TRACT 2 were either due to additions of experimentation or changes to experimentation due to results obtained from TRACT 1. The notable additions were composite subfloor retrofits for the attenuation of impact loads, and the inclusion of 4 live Emergency Locator Transmitters (ELTs) to test for activation success rate [13]. None of the experiments affected the acquisition of photogrammetric data.

The TRACT test articles were two CH-46E Sea Knight airframes acquired from the Navy CH-46E Program Office located at the Navy Flight Readiness Center in Cherry Point, North Carolina. A CH-46E was selected specifically for its large size which gave the ability to test a large variety of experiments, along with the fact that it represented a transport category aircraft in shape and design. Items not included were the engine, transmission, rotor blades, stub wings and onboard avionics. In the end, the pre-test article looked much less like a CH-46E, and much more like a generic airframe being used as a testbed. For the TRACT 1 test, the airframe was tested in its as-received, unaltered state.

TRACT 1

For each test, precise impact conditions must be gathered from the actual test results. The impact conditions need to be acquired so items such as impact velocities and pitch angle can all be known, which can then be used in describing, in part, the severity of the crash. A single 2 megapixel (MP) high-speed color camera, oriented normal to the flight path of the test article, imaging at 1 kHz. was used for the acquisition of these properties. A single camera will give information about the horizontal velocity, vertical velocity and pitch angle, which are all in-plane dimensions. The third out-of-plane velocity, along with the out-of-plane angles (roll and yaw), cannot be determined using only a single camera.

Bowtie stickers 6 in. in size were applied to specific locations on the left side of the TRACT test article. These stickers were unique and capable of being recognized by the 2-D tracking software. Each sticker represented a distinct location on the airframe. The bowtie sticker locations are identified with a yellow circle and shown in Figure 3.

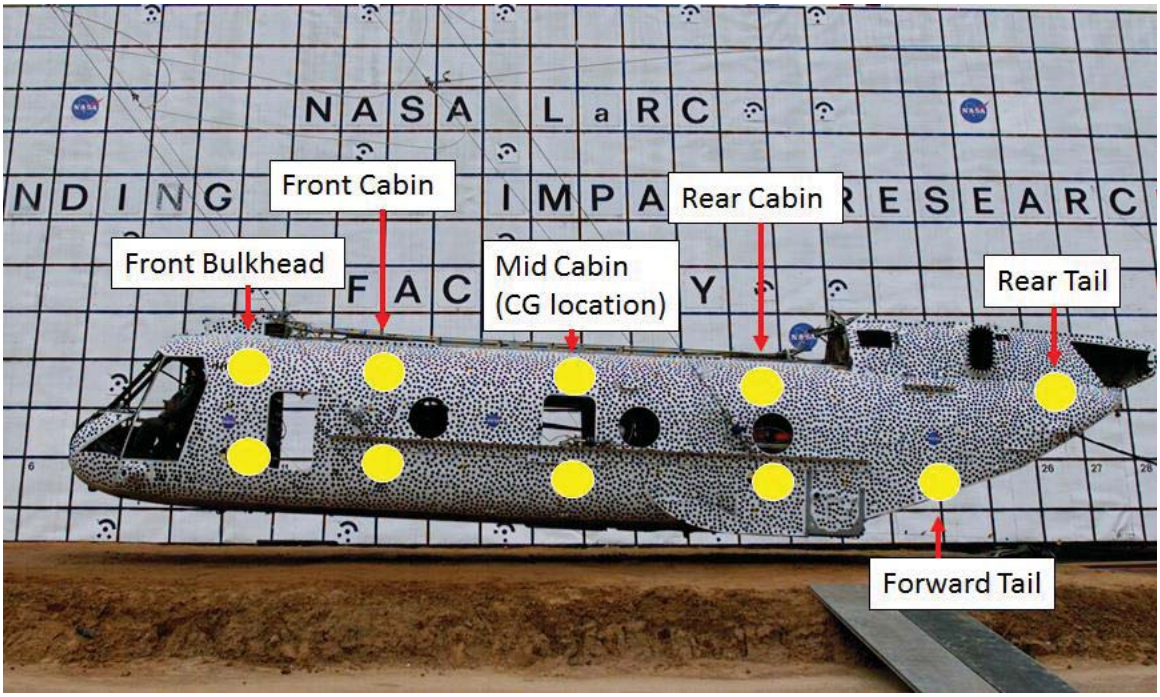

Figure 3 - TRACT 1 bowtie sticker target locations

For each identified location on the airframe, there is an upper and lower sticker, representing, for example, an upper Front Bulkhead and lower Front Bulkhead location. For reference, the CG of the test article fell between the upper and lower Mid Cabin sticker locations.

Target locations were measured prior to the test and these measurements established both a baseline target location, and also scaling factors needed in data processing. A coordinate system was established using the grid on the backboard, located behind the test article and visible in Figure 4. Figure 4 shows the created points, tracked through the time history during the crash, starting with the first tracked position, slightly before impact.

Figure 4 – TRACT 1 target tracking marker time history

The tracking algorithms used on the markers in Figure 4 started at the end of the swing, approximately 0.070 sec. prior to impact. During the final stages of the swing, the vehicle exhibited motion downward (negative Y direction) and leftward (negative X direction), which is the motion of the swing dynamics due to the pendulum swing. The markers reached a minimum, which represented the impact position, then exhibited upward and leftward motion, which represented the rebound. The distance between the minimum at impact and the relative max during the post impact arc was the maximum rebound position and grew larger when examining the data starting at the front of the airframe going to the rear. The vehicle came to rest shortly thereafter, and the location at rest is shown in Figure 4 at the final left-most point. Figure 5 shows the time history of the marker velocities, which is computed by taking the time differential of the marker positions.

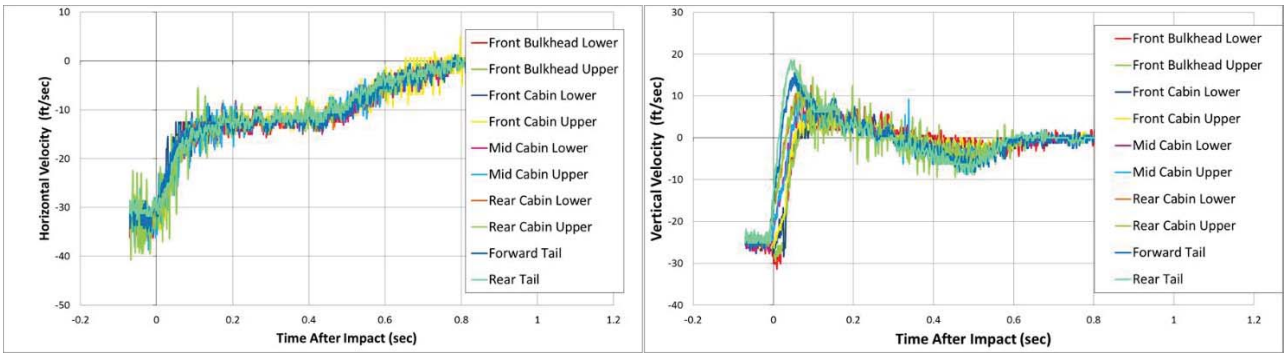

Figure 5 - TRACT 1 target tracking marker results

The impact conditions were 25.0 ft./sec. vertical and 33.0 ft./sec. horizontal velocities, as determined from the target tracking. The pitch angle was 2.5 degrees at impact. The impact velocity of the airframe can be computed from the pre-impact data shown in Figure 5 by determining the intercept location as the data crosses the time = 0.000 sec. location. Velocities were negative using the coordinate system shown in Figure 4, indicating downward and leftward motion which agrees with the tracking markers. Post-impact data show a plateau which occurred between 0.200 and 0.400 sec. in the horizontal velocity, which indicates the rebound horizontal velocity of approximately 12 ft./sec. occurring in the negative X-direction. This motion represents the horizontal velocity of the rebound of the test article. The vertical velocities show positive values indicating that rebound in the positive Y-direction occurred, with velocities ranging between approximately zero ft./sec. in the Forward Cabin, to approximately 17 ft./sec. in the Rear Tail. The differences in vertical velocities post-impact show that the vehicle also rotated, with the tail reaching the highest rebound position. The data also show that the vehicle comes to a rest approximately 0.800 sec. after initial impact, which is represented by the horizontal and vertical data crossing the zero marker on the Y-axis.

To facilitate the acquisition of three dimensional deformation data for the digital image correlation technique, the left side of the airframe was first painted white. Then, 1-in. diameter black dots were applied over the white background on the left side of the aircraft in a stochastic pattern, mimicking a random black and white polka dot pattern. The pattern was kept as random as possible by hand painting each dot without the use of a pattern. The digital image correlation software works by first grouping a set of 3-6 dots (user defined) into a pattern. After the patterns have been established, the software tracks either the rigid body motion or deformation of each grouped dot pattern and stores this information at a created point in the middle of the pattern. By capturing adjacent patterns all along the side of the airframe, a large point cloud can be computed. The point cloud can then be turned into a mesh, much like in finite element modeling. It is from this mesh of points that data can be manipulated in a variety of ways to show deformations, strains, rigid body motion, or other items of interest.

The dot patterns are captured by a pair of two 4 MP high-speed monochromatic synchronized cameras recording the crash test at 500 Hz. These cameras were located approximately 40 feet away from the test article and 30 feet apart from each other, which viewed the test article at two slightly different angles. Prior to the test, a calibration procedure was performed on the cameras [14] using the coded target array present on the backboard. The calibration procedure established scaling, relative camera location and lens distortion removal parameters. The cameras were mainly focused on the primary impact location, in which it was assumed that the main portion of the deformation on the airframe would occur. The field of view was chosen to be slightly larger than the test article; however, the field of view was only capable of measuring about 8 feet of the slide-out distance. Prior to the test, the slide-out of the vehicle was unknown.

The TRACT test article proved to be a good candidate for the resolution of the digital image correlation results. Since the painted side of the fuselage offered a large continuous surface area, a large amount of data could be resolved. Even with the large surface area, there were spots which were intentionally uncomputed due to test constraints. For example, the two areas behind the main swing cables separated from the TRACT test article swing hardware were not computed. These areas were ignored due to the perceived large amounts of motion which could have occurred from the dynamic cable motion over the static dot pattern at these locations.

Figure 6 shows the deformed time history from the lateral deformation experienced on the airframe at four notable times during the crash test.

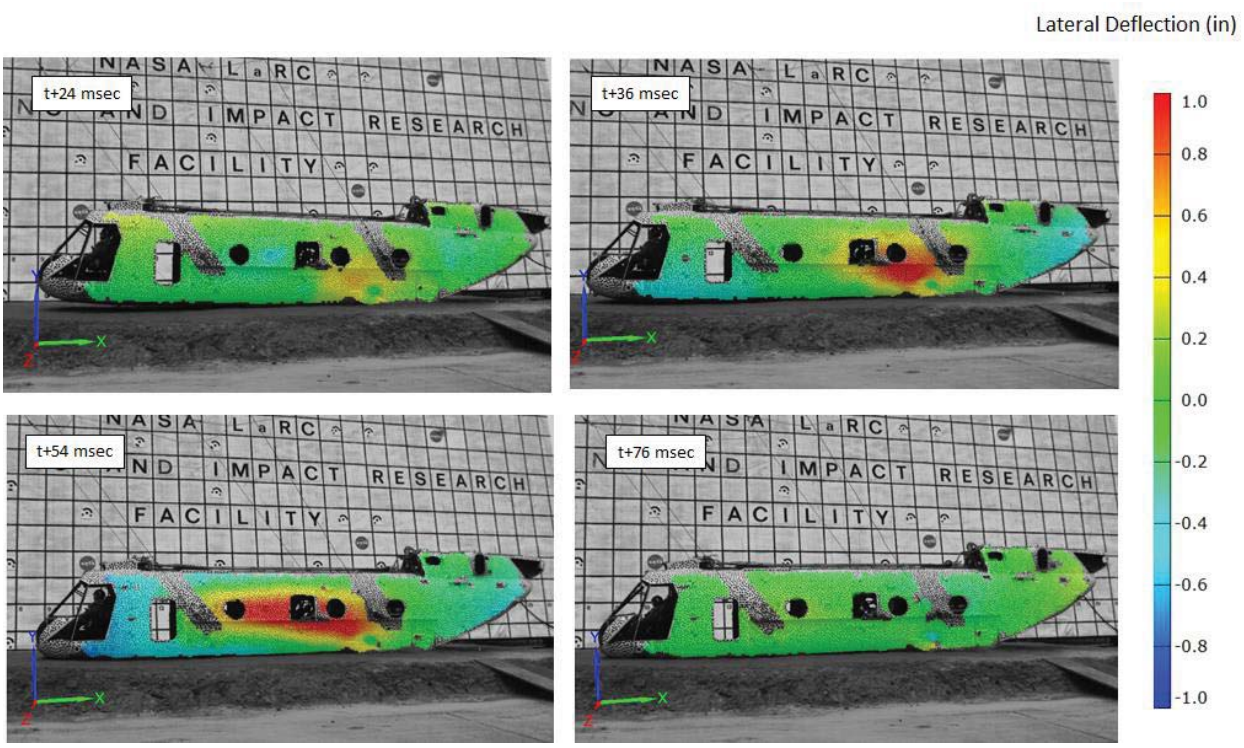

Figure 6 - TRACT 1 full field lateral deflection plot

Figure 6 shows four different deflection plots of the TRACT 1 test article, and shows a large lateral deflection developing 0.024 sec. after initial impact in the lower rear portion of the test article, near the stub wing attachment location and immediately in front of the non-computed area at the rear swing cable. At 0.036 sec. after impact, the deformation reached approximately 1 in. in magnitude and began traveling higher and forward of the initial location, heading toward the Mid Cabin location. At 0.054 sec. after impact, the largest area of deformation was seen at the Mid Cabin location. All of the deformation dissipated 0.076 sec. after impact, indicating a mostly elastic response from the airframe in the lateral direction.

Knowing the behavior of the airframe presented above, individual points were interrogated for further examination, which are shown in Figure 7. These points corresponded to the bowtie sticker locations used in the two dimensional impact condition analysis. A digital extensometer was created between the upper and lower portion and a relative deflection was examined. The extensometer measured the distance between the two picked endpoints, and divided the distance by the original undeformed distance, much like what is measured with a conventional strain gage.

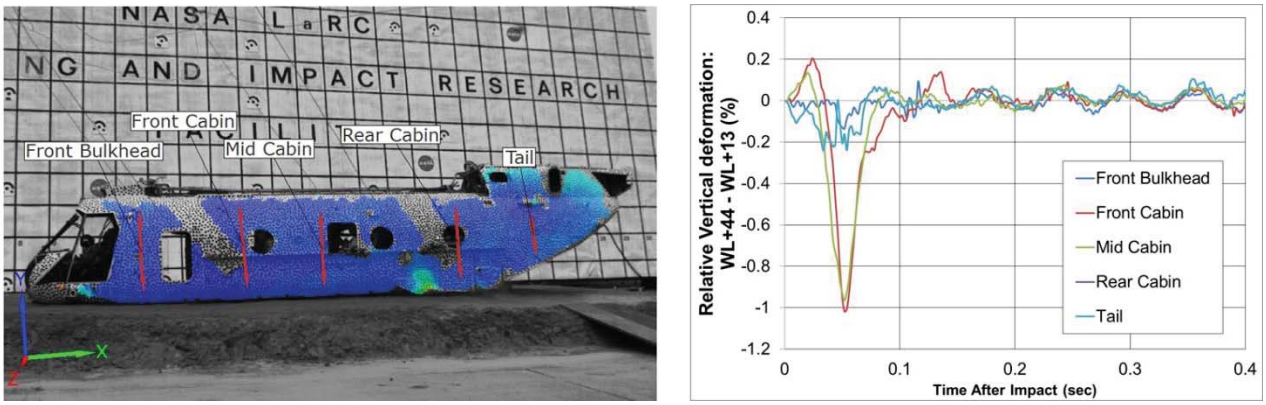

Figure 7 - TRACT 1 relative vertical deformation

The vertical deformation was most pronounced in the Mid and Front Cabin of the airframe, which was where the largest unsupported portion of the airframe was located. The deformations reached approximately 1% deformation 0.050 sec. after impact, and then track back toward zero and mimic the responses from the other locations after 0.015 sec. after impact. After 0.015 sec., the oscillations which occurred were from the airframe flexing due to the initial impact while in the air. The large deformations which appear in the Front and Mid Cabin were elastic deformations.

The airframe, as noted above, sustained a relatively elastic impact. There were, however, areas of permanent deformation, as determined by examining the airframe strain from a time that was well past initial impact with the ground. Figure 8 shows permanent strain on the airframe during the rebound event.

Figure 8 - TRACT 1 permanent deformation

The main areas of permanent strain were present on the stub wing structure, mainly where the initial impact occurred at the rear of the airframe. Another area of permanent deformation was in the cockpit, right below the pilot location. This deformation was likely due to the "slap down" effect, which occurred at the front structure impacting the surface with higher vertical velocity due to the rotation, or slap down, of the front of the aircraft about the rear impact area. Other locations that showed high deformation were around the structure supporting the swing beam, needed for lifting and hoisting of the airframe for the test. There is a good possibility these strains were spurious due to the swing beam/airframe attachment configuration. There was some freedom for the swing beam to move relative to the airframe structure, and thus would register erroneous strains. The strains around this area were also ignored. Also note that the slide-out of approximately 8 feet was mostly within the camera field of view, with the only exception being the front of the nose of the test article. The permanent strains on the nose of the test article were unable to be tracked due to their position out of the field of view, and are unknown.

TRACT 1 also contained 7 onboard high-speed cameras focused on the onboard occupant motion. These cameras were 1 MP either color or black and white, and recorded the impact at 500 Hz. All of the cameras were mounted in ruggedized enclosures and fastened to hardened points on stiffeners along the roof of the airframe. Each camera tracked the in-plane motion of either one or two occupants, creating a two dimensional solution. A simple calibration was completed prior to the test by placing a panel with scale bars into each plane of motion needed to be tracked. Figure 9 shows the calibration performed on one of the ATDs; in this case, the 5th percentile Hybrid 3 (HIII) ATD in a forward facing seat. The calibration panel contained a target array arranged in various sized box patterns. Using the boxes and knowing the scale between the targets, a perspective calibration was completed which corrected for the angle difference between the camera and plane of motion. A perspective calibration was utilized because it removed the requirement for the camera to be perfectly normal to the plane of motion. For cameras containing multiple ATDs in view (like what is seen in Figure 9), the panel was placed in the planes for both occupants, creating separate calibrations for each.

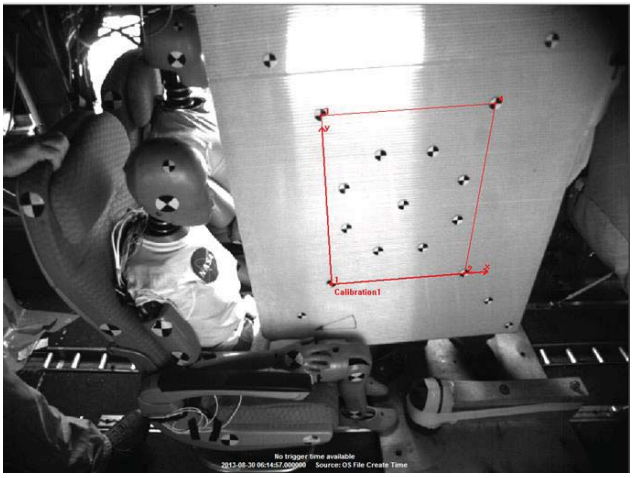

Figure 9 - Example onboard 2D calibration used in occupant tracking

Using the tracked targets on the seat back, armrest, ATD head, right arm and right leg, the motion of the ATD was tracked and a flail envelope was established. Figure 10 shows the fail envelope of the head, which was found by determining the relative position between the seat back and the ATD head. Figure 10, left, shows the tracked markers, while Figure 10, right, shows the resolved data trace.

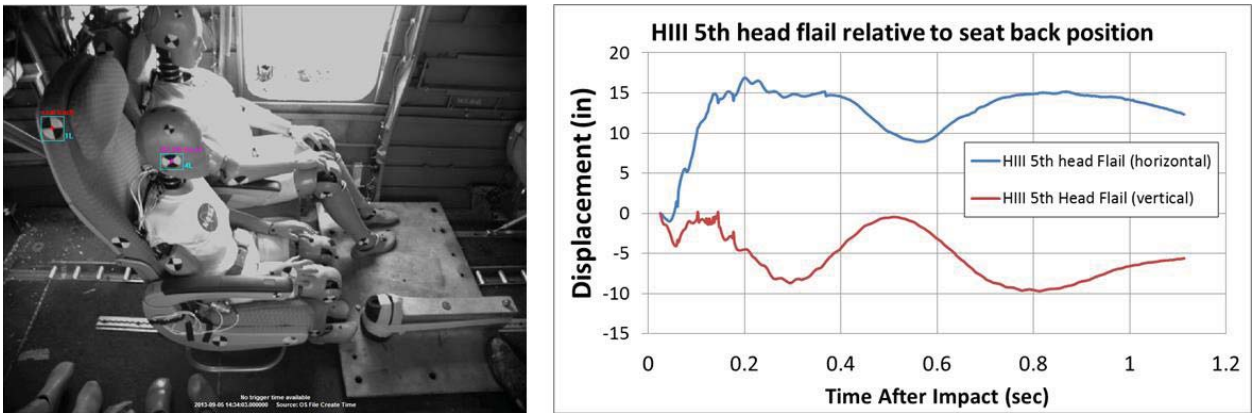

Figure 10 – Example ATD motion tracking during TRACT 1 test.

The maximum horizontal flail for the head was 16.5 in., which occurred 0.200 sec. after impact. The head then reached a relative minimum of 9.0 in. at 0.569 sec. after impact, and afterward proceeded toward a second maximum of 15.1 in. at 0.857 sec. after impact. In the vertical direction, the head reached a relative maximum downward displacement of 8.7 in. at 0.299 sec. after impact. The head nearly rebounded to an initial position of 0.5 in. at 0.515 sec. after impact. The largest tracked vertical motion of the head occurred at 0.802 sec. after impact, which reached a maximum downward vertical displacement of 9.62 in. The existence of the two peaks in both data sets is attributed to the initial impact of the airframe and the subsequent rebound and second impact. Similar analyses were performed on the other ATDs using the video acquired from the other onboard cameras.

A sensor with markerless tracking capabilities was also placed onboard to track the motion of one of the onboard ATDs. Hardware developed for the commercial gaming industry to track player motion during gameplay was utilized to determine whether it would be possible to track ATD motion and subsequent flail envelopes during impact. The fundamentals behind the motion tracking lend itself well to the tracking of ATD motion. The basic understanding behind the sensor's characteristics is presented.

The sensor functions by utilizing a color camera and an infrared camera in conjunction with a projected infrared dot grid. An infrared dot grid is normally invisible unless examined with certain types of infrared cameras. The spacing between all dots in the grid field is known for particular distances, ranging from approximately 0.4 to 4 meters in its normal range. If an object steps into the sensor's field of view and interferes with the dot pattern, the spacing will change. The dots will appear further apart at closer distances, and closer together at further distances. An infrared camera can see the dot spacing, and the information from the dot spacing obtained by the camera is stored in a global distance matrix, which measures the distance for dots appearing in every pixel of the camera. Figure 11 shows an example of the projected infrared dots, both from a far-away perspective (left) and from a close-up perspective (right).

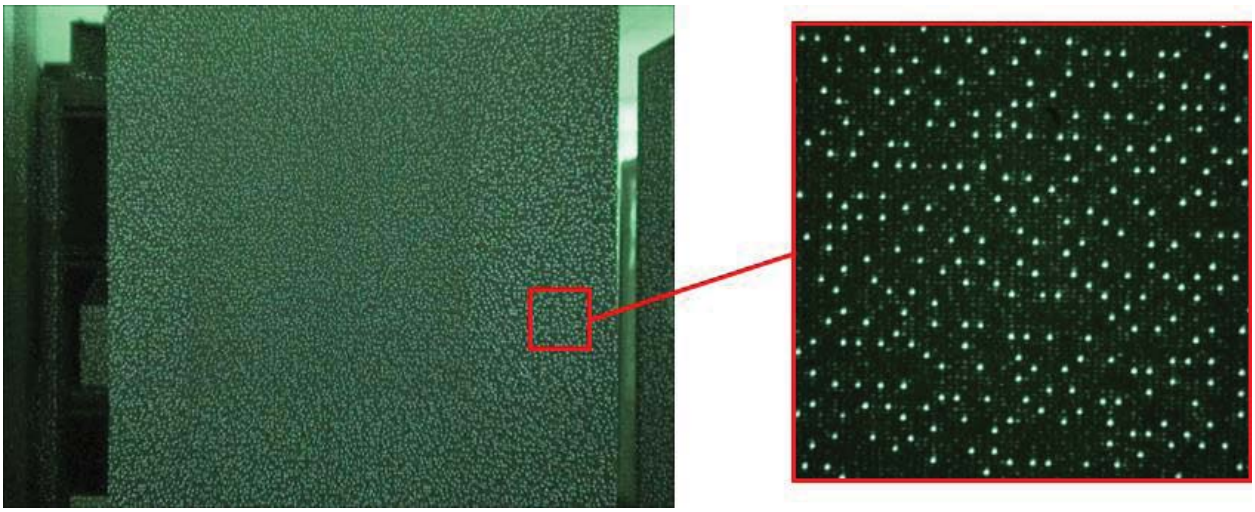

Figure 11 - Markerless tracking projected infrared dot field

There is internal logic present inside the sensor to detect whether an object in the field of view is "human" in shape. It will attempt to create a wireframe overlay onto the object in the field of view. The wireframe is comprised of a stick figure representation of a human form, with intersections of particular appendages stored as joints. The sensor will then attempt to track the joint motion in real time to determine position and motion which is normally used to control gameplay. However, by using the sensor capabilities along with a commercially available software development kit and custom programming, it is possible to track and store the joint position data in 3-D space. When coupled with an ATD, which is representative of a human shape, it is possible to use the sensor to track and store ATD motion. It is from the tracking and storing of the joint data that information about occupant deformation, flail envelopes, and other responses seen in the impact can be analyzed. Figure 12 shows early checkout tests conducted on one of NASA ATDs, complete with resolved green wireframe stick figure overlay for a demonstration of proof of concept. The joints are in light green where two "sticks" meet.

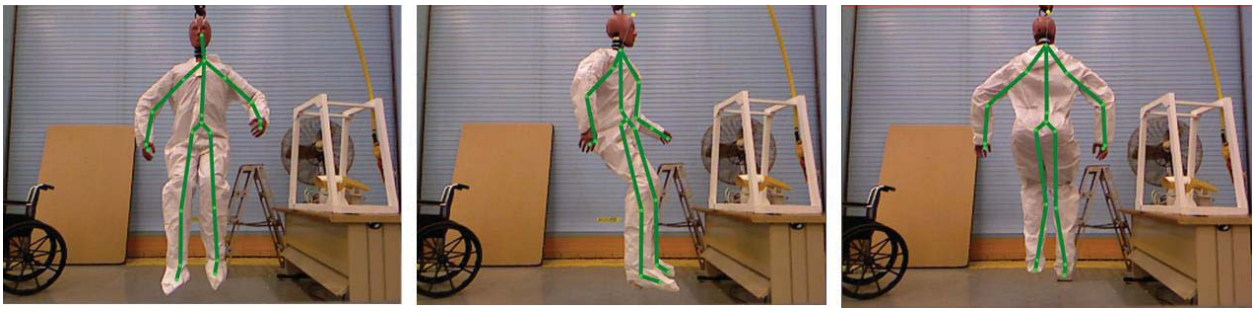

Figure 12 - ATD Markerless tracking proof of concept testing

The sensor was placed on the TRACT test article in a forward bulkhead near the floor, underneath the front portion of the data acquisition systems (DAS), focused on left side standing ATD, as shown in Figure 13. The particular ATD contained a large amount of simulated combat gear, needed for ballast, along with uniform and helmet (not shown). It was instrumented with various sensors, and the cabling from the sensors was routed behind the ATD, up to the ceiling and then into the front DAS. The ATD was located approximately 4 feet away from the sensor location.

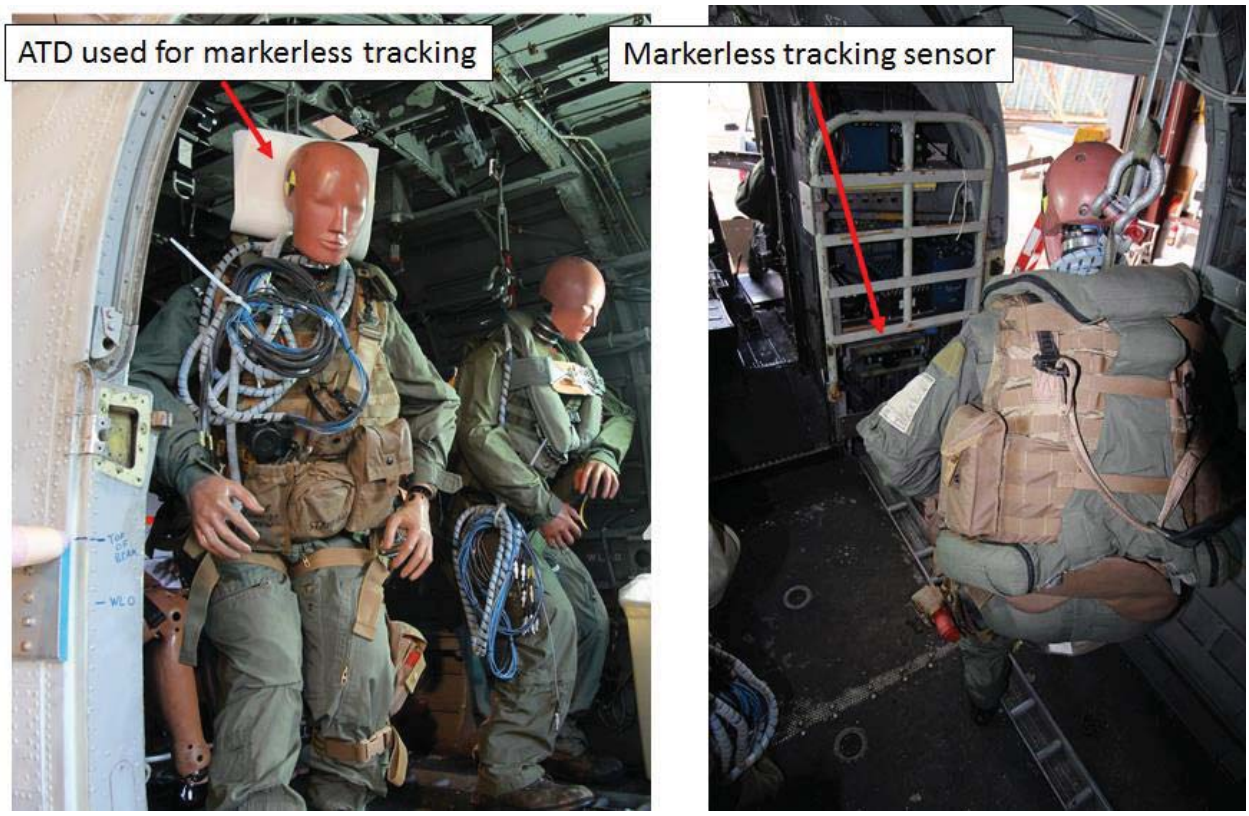

Figure 13 – TRACT 1 ATD used for markerless tracking

The sensor was able to obtain limited amounts of 3-D position information, which is shown in the false color plots in Figure 14. It is hypothesized that the large amount of infrared energy originating from the outdoor conditions of the test obscured the sensor's internal infrared projection grid. The wireframe overlay was also not able to be tracked. Due to a limited portion of the available depth data and the additional items present on the ATD, the algorithms determining the presence of a human form did not accurately identify and generate the joint data.

Secondly, the sensor was only able to track the motion during the swing aspect of the test, which occurred prior to the impact. At impact, the large amounts of motion resulting from the crash caused the ATD to kick the sensor out of its mount, thus making it unusable for any post-test data analysis. However, the fact that even a partial data set was able to be captured was encouraging. Figure 14 shows a time history of the data available from the markerless sensor, with the left sequence showing images captured from the color camera, and the right sequence showing the depth data color-mapped into a plot image.

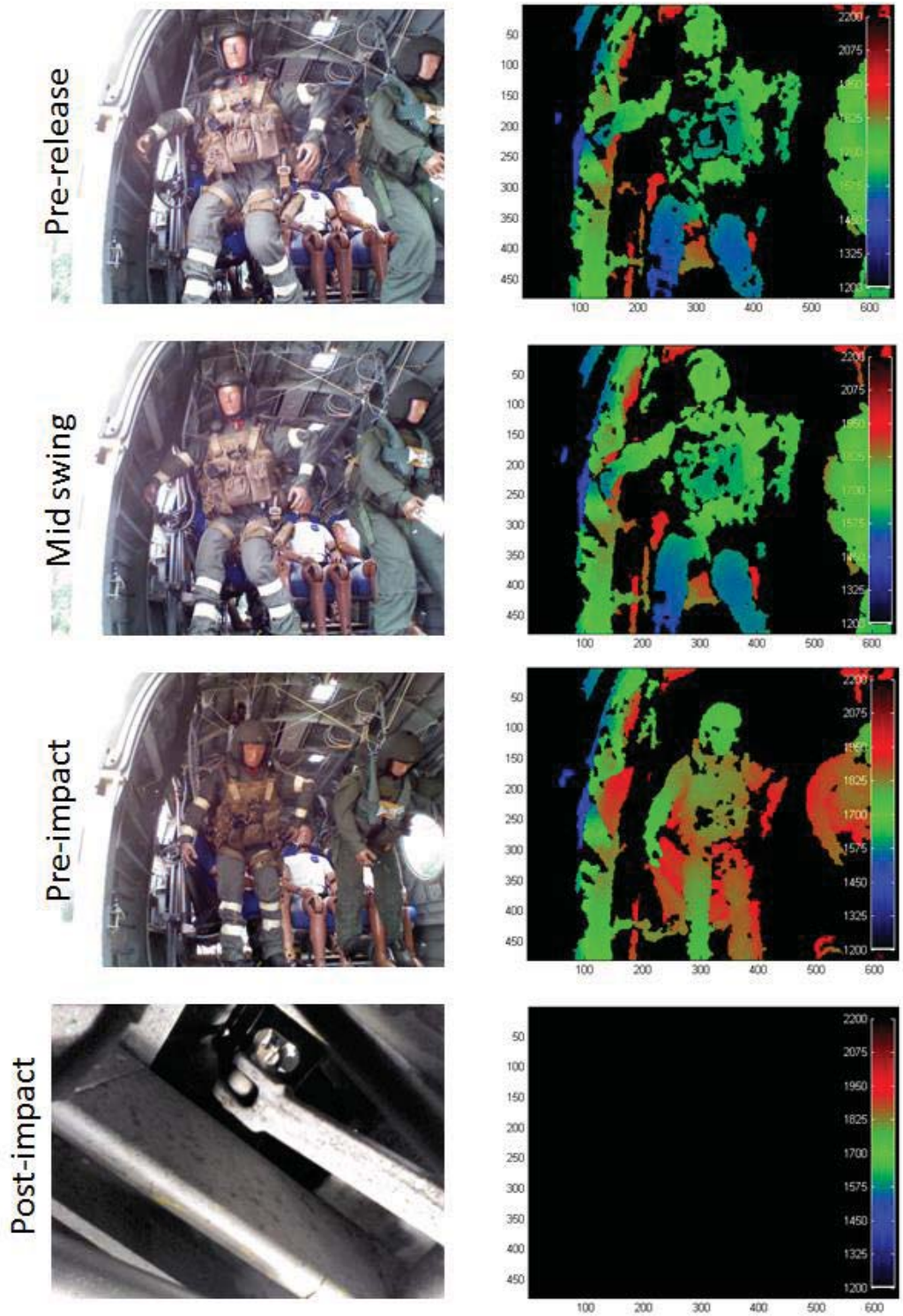

Figure 14 - TRACT 1 markerless tracking results. Visible image (left) and created depth data projection (right)

The effective range for displacement measurements obtained from the markerless sensor used on the TRACT 1 test was between 47.24 and 86.6 in. (1.2 and 2.2 m.). Items in the field of view closer than 47.2 in. and further than 86.6 in. appeared black in the area surrounding the tracked ATD. The ATD, prior to impact and swing, was originally positioned near the middle of the measurement range, at around 66.92 in. (1.7 m.), as denoted in green. The crouch of the ATD caused the legs and knees of the ATD to appear closer to the sensor at approximately 57.09 in. (1.45 m.), which is designated in blue. As the test article began swinging forward (the pre-impact images), the momentum of the ATD caused it to move backward, reaching the far end of the sensor's displacement range of between 71.95 and 81.69 in. (1.825 and 2.075 m.) Due to the nature of how the sensor tracked spatial depth through the use of a statically projected dot pattern, individual point tracking was not possible.

TRACT 2

As previously stated, TRACT 2 experimentation closely mimicked TRACT 1 experimentation with the exception of notable additions or changes.

Two-dimensional impact condition tracking was also completed on the TRACT 2 test. Similar targeting methodology was used, placing 6-in. bowtie stickers in locations starting in the Forward Bulkhead and extending back out to the Tail. As with TRACT 1, target locations were measured prior to the test and these measurements established both a baseline location and scaling factors needed for data processing. A coordinate system was established using the backboard located behind the test article and visible in Figure 15. Figure 15 shows the created points, tracked through the time history during the crash.

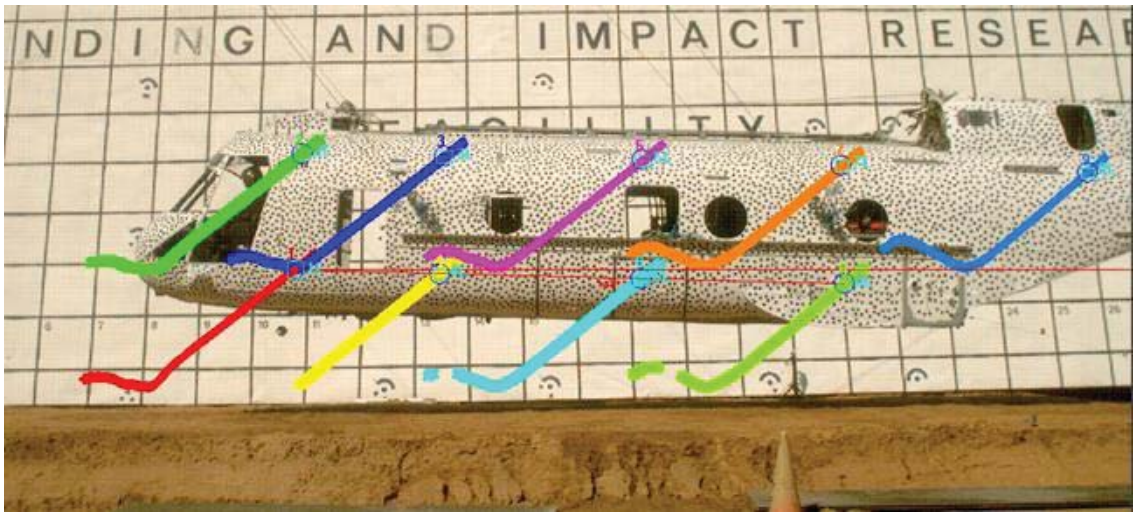

Figure 15 - TRACT 2 target tracking marker time history

The 2-D impact data showed the test article impacted at 33.7 ft./sec. horizontal and 25.4 ft./sec. vertical velocities. The pitch angle was 2.6 degrees at impact. The two dimensional tracking data showed a remarkable difference in results when comparing the horizontal velocity results post-impact. The TRACT 2 test article showed a noticeable difference in post-test horizontal velocity, reaching a zero horizontal velocity approximately 0.53 sec. after impact, which represented the test article coming to rest. Conversely, the TRACT 1 test article motion lasted approximately 0.3 sec. longer, with the TRACT 1 test article finally

coming to rest at a time of 0.83 sec. after initial impact. These results correspond to post-test slide-out measurements. TRACT 1 exhibited approximately 96 in. of slide-out, while the TRACT 2 test article only exhibited 51 in. of slide-out. This difference in horizontal velocity time histories was important because it was the first indication that the horizontal deceleration on the test article was much higher for TRACT 2. Figure 16 shows a comparison of the velocities between the TRACT tests.

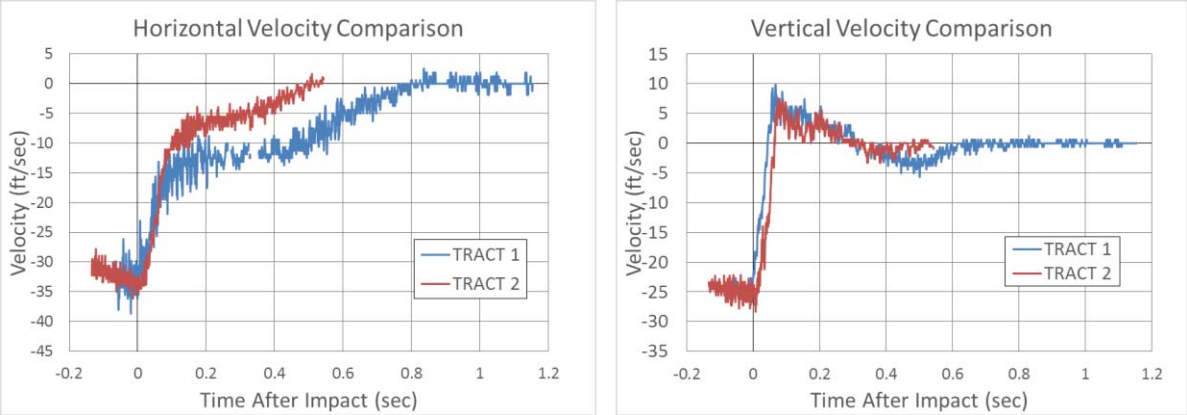

Figure 16 - TRACT 1 to TRACT 2 velocity comparison

Differentiation of the horizontal velocity data showed the average accelerations between 0.200 and 0.500 sec. after impact to be higher in TRACT 2 than in TRACT 1. In the vertical direction, the velocities matched well. The velocity results suggested that the dirt compression did not have a noticeable effect on the vertical motion, however the shearing motion of the test article on the dirt did affect the horizontal motion.

An image sequence of the TRACT 2 test is shown in Figure 17. The airframe clearly exhibited a different response than in TRACT 1. At 0.028 sec. after impact, the lateral deflection started to resemble the outward lateral deflection seen in TRACT 1. The lateral deflection started to move toward the front of the airframe, a shear failure in the Forward Cabin caused the lateral deflection to dissipate, and caused the nose to experience negative (away from the camera) lateral deflection at 0.048 sec. after impact. However, when the cockpit impacted the soil at approximately 0.090 sec. after impact, it experienced positive (toward the camera) lateral deflection. There is a large positive-to-negative lateral deflection gradient going from the front to rear of the airframe.

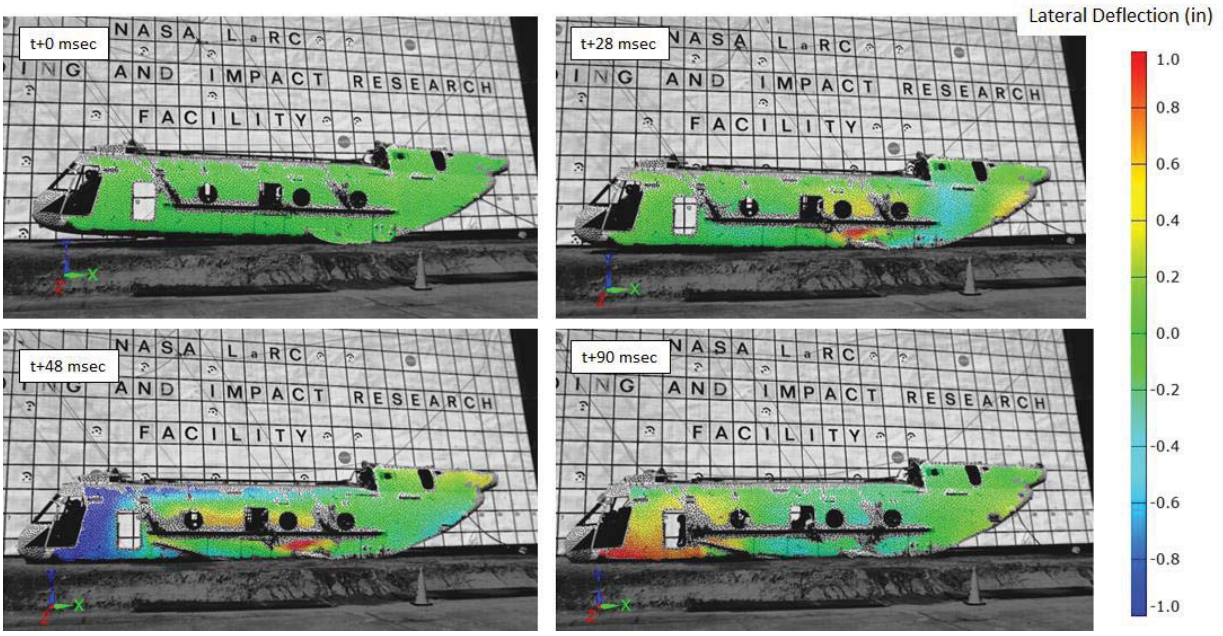

Figure 17 - TRACT 2 full field lateral deflection plot

The large gradients on the airframe shown in the lateral deflection plots suggest that a large amount of strain occurred during the test. As with TRACT 1, line strains are next plotted for five distinct areas along the airframe. These quantitative values for the airframe strain are shown in Figure 18.

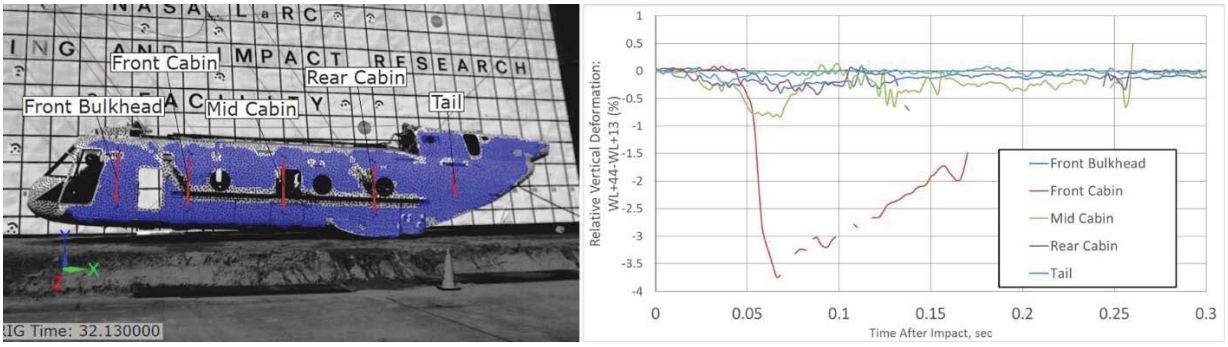

Figure 18 - TRACT 2 relative vertical deformation

The line strains show that the vast majority of the deformation occurred around the Front Cabin area, with residual effects at the Mid Cabin area. There was a large amount of data dropout from the Front Cabin area due to the large shearing failure which obscured the dot pattern near the bottom point location of the measurement. However, the maximum value of 3.74% was tracked and occurred at 0.056 sec. after impact. The two closest plotted positions nearest to the failure were the Front Bulkhead and the Mid Cabin locations. Both of these locations suggested permanent airframe deformation, resulting from a small negative value of relative deformation after 0.056 sec. The Front Bulkhead data ranged between 0.07% and 0.17%, while the Mid Cabin data reached almost 0.35% relative deformation after the airframe shear failure.

The data agreed with the visual inspections of the airframe, which clearly showed a skin shear failure. One advantage of the digital image correlation data is that any point along the airframe can be investigated. A digital extensometer was applied to the endpoints forward and aft of the failed region. Figure 19 shows a picture of the created extensometer on the left, and the plotted data on the right.

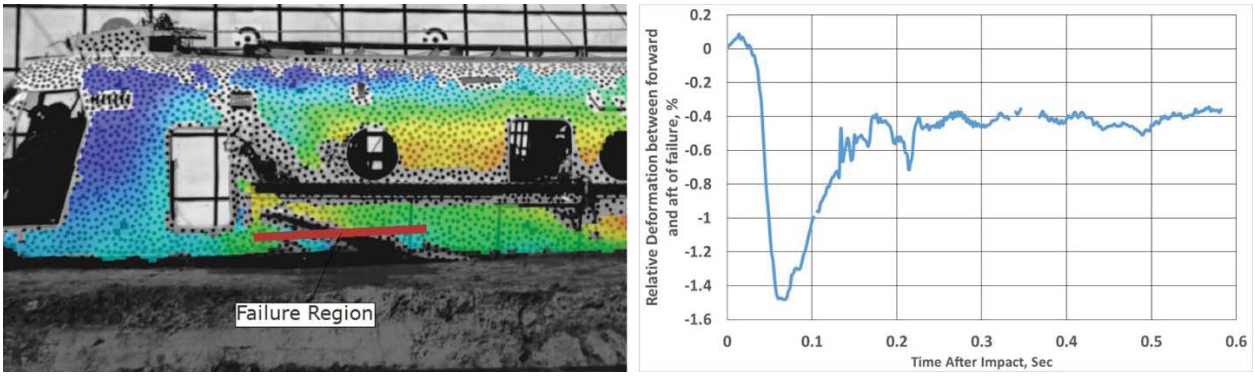

Figure 19 - TRACT 2 strain across failure region

The maximum compressive strain is 1.48% and occurred at 0.062 sec. after impact. The compressive strain deviates from this peak value to approximately 0.4% for the duration of the impact sequence. The 0.4% strain was the permanent deformation resulting from the shear failure seen in the skin.

Similar analyses were conducted for the onboard occupants using videos acquired from onboard cameras. For TRACT 2 there were 5 additional high-speed cameras used, giving an onboard camera total of 12. There was at least one camera focused on each of the ATDs, along with cameras focused on other onboard experiments. One experiment, a composite retrofit subfloor [15], was imaged through a window created in the floor. The purpose of tracking the subfloor was to examine the crush behavior during the full-scale crash test and compare it to previous subscale and full-scale drop tests. Figure 20 shows the composite subfloor through the window in the floor.

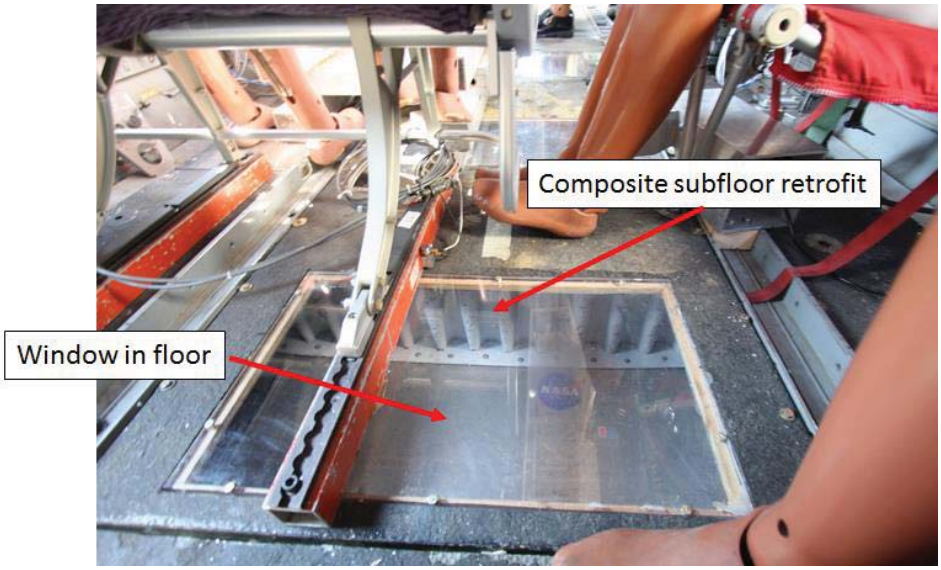

Figure 20 - TRACT 2 subfloor

An existing frame section was removed and the composite subfloor was retrofit into its location for the evaluation of energy absorbing characteristics. The subfloor was located at the frame location where a forward facing seat with the ATDs was positioned. A small 24-in. by 24-in. piece of the original floor was removed and a ½-in. thick polycarbonate sheet was installed in its place. A black and white high-speed camera was positioned onto the data collection shelf located approximately 2 ft. behind the floor section and approximately 2 ft. above the floor. The angle of the camera allowed it to see approximately 3 ft. (out of a total of 8 ft.) of the length of the floor. Figure 21 shows an image sequence of still frames obtained from the high-speed video. The composite subfloor was illuminated from an under floor lighting system. The composite subfloor was also painted white, and black tick marks were applied every 3 in. in the vertical direction to aid in crush tracking.

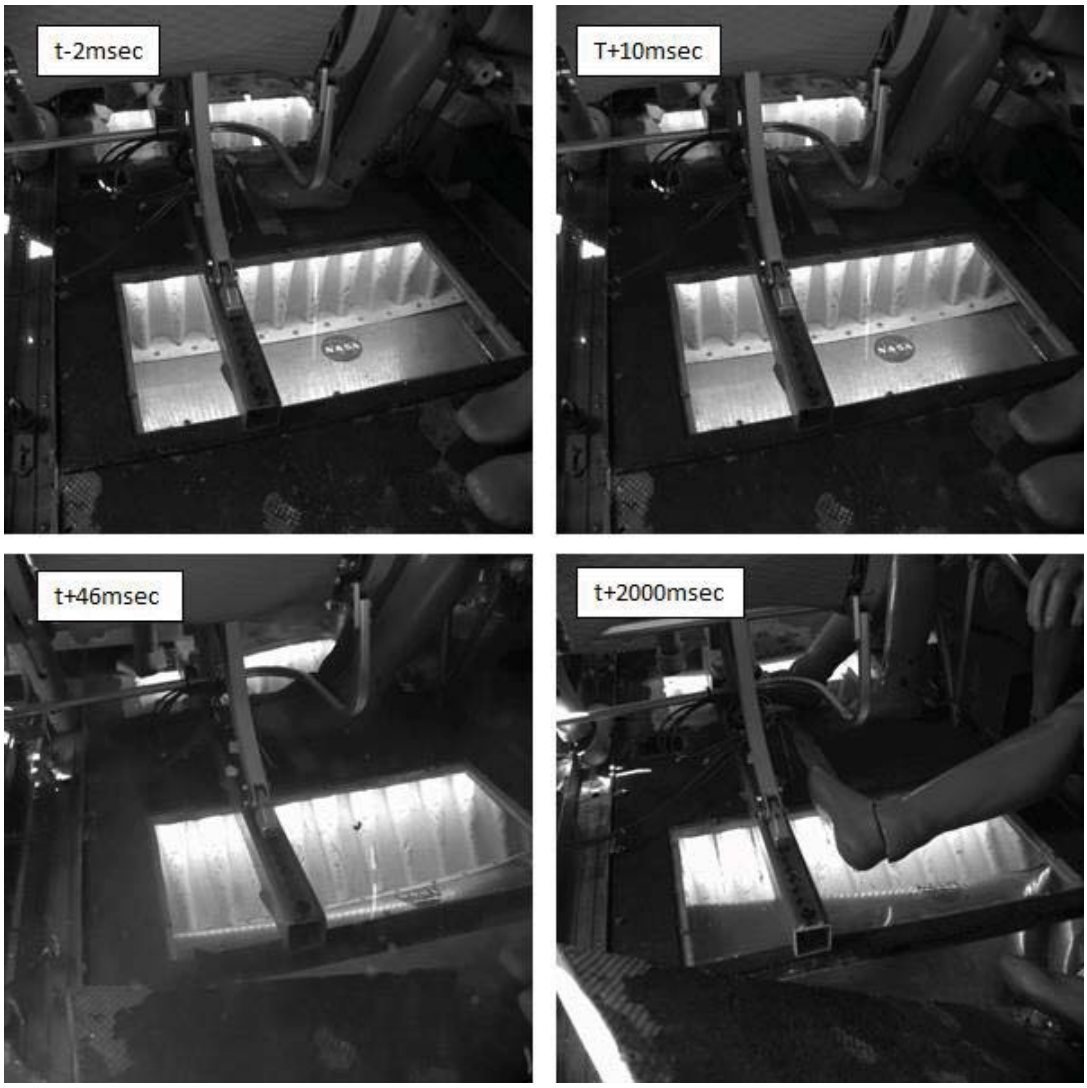

Figure 21 - TRACT 2 composite subfloor experiment

The upper left image in Figure 21 shows the subfloor immediately prior to impact. A portion of the subfloor can clearly be seen through the window, signifying that the subfloor is intact during the swing, and is pristine for use in the impact. The upper right figure shows the subfloor 0.010 sec. after impact,

immediately after the rear portion of the test article has impacted the soil. The lower left image shows the subfloor at 0.046 sec. after impact, which is the time where the shear failure developed in the forward cabin. The shear failure is seen in this image, noting that the subfloor has not crushed, but rather exhibited deformation by rotating backward due to the shearing motion. The bottom right image shows the subfloor 2.000 sec. after impact, after the motion has stopped. Large amounts of subfloor deformation, along with the deformation along the actual floor of the test article are shown. Unfortunately, the shearing of the composite subfloor did not allow for it to crush as intended, but data generated from the camera images; which showed the precise motion of the floor during the impact, are remarkable.

A similar setup from TRACT 1 was used for the markerless tracking sensor on TRACT 2. It was placed in a forward bulkhead, and focused on one of the standing ATDs. For TRACT 2, the standing ATD experiment called for the ATD to be facing backward, making the face not visible to the markerless tracking sensor. A cage was built around the sensor, and its mounting bracket was stiffened such that it could retain its field of view throughout the crash sequence. The acquired results are shown in Figure 22.

22

Figure 22 - TRACT 2 markerless tracking results. Visible image (left) and created depth data projection (right)

The markerless tracker acquired a larger time history of motion than TRACT 1, however data dropout was still persistent on the ATD. The sensor was able to obtain limited amounts of 3-D position information, however areas around the upper back where a backpack was located did not get tracked at all. The head also did not get tracked, mainly due to the backpack obscuring the grid projection onto the head. However, the arms and legs are clearly visible in the depth data. The wireframe overlay was also not able to be

tracked due to these reasons. Overall, the results were of the same quality of the TRACT 1 results, and were of limited use during post-test data analysis.

The added protection enabled the sensor to obtain results during and post-impact. Blurring from the visible camera occurred both during and after the impact, which possibly affected the depth data. The sensor seemed to freeze approximately 0.100 sec. after impact. There were two main hypothesized reasons why this occurred. The first was that the data cabling between the sensor and the processing computer became loose. However, as this cable was a part of a bundle containing other DAS and camera data originating from the aircraft into the LandIR control room and all other cables were still intact, this idea was dismissed. The likely reason was that the sensor was unable to withstand the high impact accelerations associated from the crash event. If the sensor is to be used for future testing, it will need to be mounted in a rigid manner but also contain some energy absorbing structure for protection. Additionally, it will need to be shielded from ambient light to allow it to capture more depth-of-field data.

ELTSAR Test Series

The ELTSAR crash tests were conducted during the summer of 2015. During this time, three Cessna 172 aircraft were crashed with the main objective of evaluating the system performances of onboard Emergency Locator Transmitters (ELTs) under severe but survivable realistic crash conditions. The three tests simulated three different crash conditions and the full suite of results including aircraft acceleration response, ELT performance and onboard occupant injury are fully documented in references 16 and 17. However, a brief overview is provided for background information.

Three differing crash scenarios were evaluated for the test series. The first scenario represented a flare-into-stall emergency landing onto a rigid surface such as a highway. This scenario was tested by impacting the airplane onto concrete featuring a high sink rate at a slight nose up attitude. The second and third scenarios were impact tests onto a soil surface. This surface was created by building up a 2-ft. high bed of soil at the impact location. In scenario two, the airplane impacted the soil in a nose down attitude, simulating a Controlled Flight Into Terrain (CFIT). In the third scenario, the airplane impacted the soil in a nose up attitude, resulting in a tail strike condition. The experimental suite was much smaller for the crash tests of three Cessna 172s, mainly due to time and space constraints. However, the pilot side of each airplane was painted with a stochastic speckle pattern, with 0.75-in. black dots being painted onto a white background. The full field photogrammetry data analysis would hopefully determine airframe deformation, identify weak spots which could be improved, and in general, acquire previously unknown response data from a Cessna 172 airframe during a crash condition.

The camera setup for the ELTSAR test series was similar to that of the TRACT tests. For 2-D tracking, a single 2 MP color high-speed camera, imaging at 1 kHz., was located approximately 40 feet away from the airplanes, and oriented normal to the flight path. The lens was chosen such that it encompassed the entire airframe and immediate surrounding area, creating a field of view slightly larger than the airplane itself. However, there were field of view concerns, and they will be addressed in the *Data Interpretation Limitations* section.

For 3-D tracking, two 4 MP monochrome cameras sampling at 500 Hz. were located 40 feet south of the test article. Each was angled at approximately 15 degrees toward the center of the airplane, such that the total angle between the cameras was 30 degrees.

Due to limitations of space onboard each airplane and time required for photographic experimental development, the data which will be presented in the following sections will only feature setup and results from the 2-D impact conditions and digital image correlation measurements using either 2-D or 3-D techniques.

Data Interpretation Limitations

The ELTSAR test setup made data collection and interpretation challenging. Unlike the TRACT tests, where the fuselage was a 47-foot long, 8-foot tall generally rectangular (when interpreted in a profile view) object which offered a lot of coverage for data acquisition, the coverage area on a Cessna 172 was much smaller and geometry of the airplane made data interpretation much more complex.

Cessna 172 general dimensions are approximately 24 feet long from propeller to tail, and 8 feet tall at the top of the tail. The tail side profile is only a few square feet when examining the taper in the height with the length, with the vertical stabilizer giving the largest side profile surface area. The horizontal stabilizer serves to divide the long tail and the vertical stabilizer from a continuity of data collection standpoint, meaning that the painted surface is physically separated by the stabilizer. The nose and cabin offer a relatively large amount of surface area, however with the windows at the top of this area, and the wing strut dividing the area into the nose and the cabin (when viewed from a side view camera), this profile quickly becomes scattered into much more compact areas.

The coverage issues are compounded due to the dynamic nature of crash testing at speeds approaching 30 to 40 knots, which are in the range of the stall speed of a Cessna 172. The impact location is determined prior to impact which removes one variable from test, however the the events which will happen once the airplane has impacted the ground is always unknown, which makes camera placement and lens selection difficult. In two instances presented in the paper, the data captured the initial impact and part of the initial slide out, but was unable to cover the rotation of the aircraft due to field-of-view limitations. Luckily, the results showed the main deformation of the aircraft was captured before the rotation occurred. Figure 23 demonstrates the placement for cameras typically used, and Figure 24 demonstrates that the results are sometimes not anticipated when conducting dynamic crash tests.

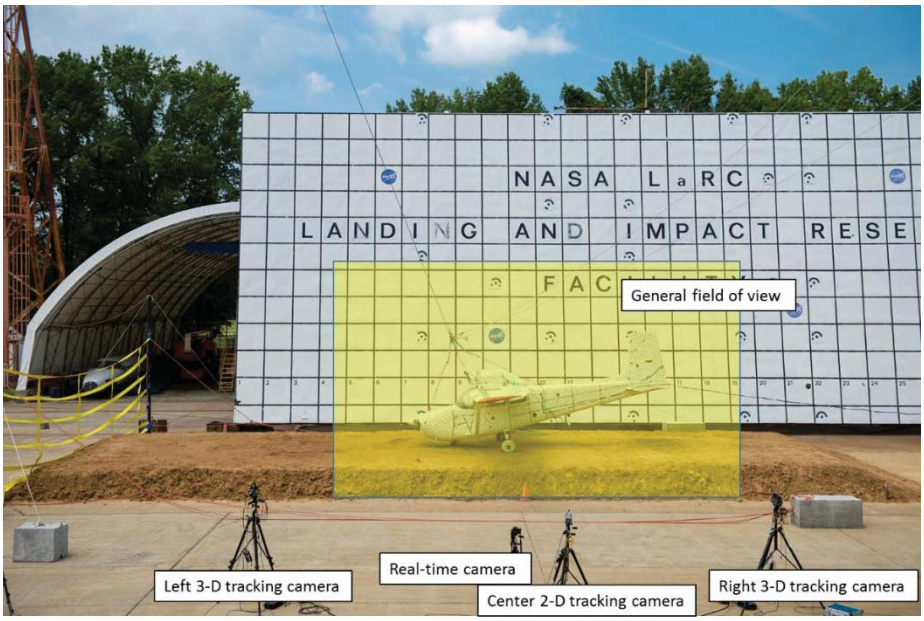

Figure 23 - General field of view for 2-D and 3-D tracking

For example in ELTSAR Test 2, it was unknown whether the airplane was going to plow into the soil surface and stop immediately, touch and skip off the soil surface with a large amount of horizontal velocity, or flip over and land in some unknown post-test location. Engineering judgment must be used to balance the competing requirements to focus on the particular impact location to gather the most amount of detail, or to zoom out to a much wider area, which may or may not be used. The field of view cannot be simply made as large as possible because details from the crash become lost, and the bowtie targets and dots on the dot pattern become too small to track. Figure 24 shows the camera field of view highlighted, along with the test sequence, and how the airplane landed just left of the focused field of view.

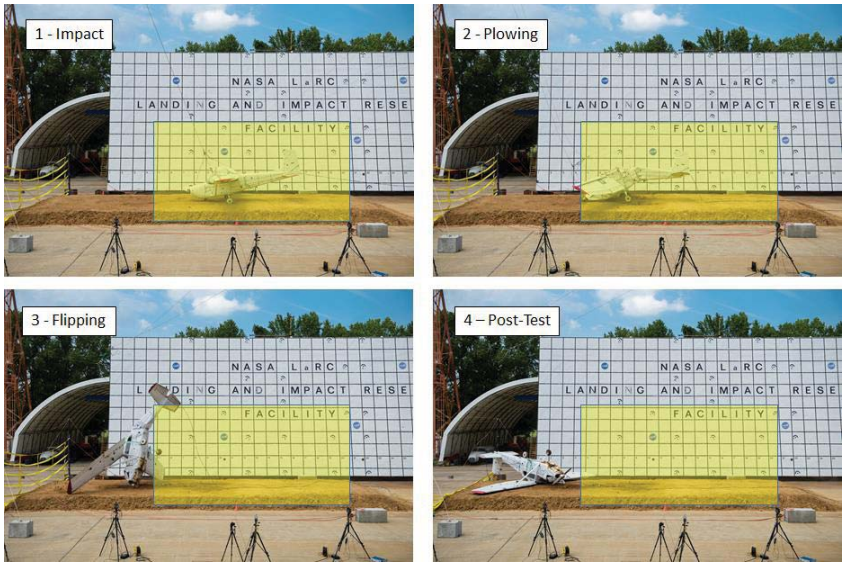

Figure 24 - Example of field of view limitations (ELTSAR Test 2 shown)

Fortunately, there were enough additional cameras available. Some were specifically focused on the yellow catch net from different angles and were able to capture the airplane flipping. However, quantitative data analysis was very limited, so these cameras were more qualitative in nature, and the only quantitative data from the test was generated from the yellow highlighted area.

Furthermore, the constraints of the specific test articles are a third factor which affected the resolved photogrammetry results. Since a Cessna 172 is a high wing aircraft, there is a stabilizing strut which connects the wing to the lower portion of the cabin, forward of the doors. This strut creates a discontinuity in coverage, which is compounded when examining the strut location from slightly different camera angles, needed for a 3-D solution. The strut now appears to give two unresolved areas of coverage due to the differences in views from the two cameras. Additional obstructions in the dot pattern are attributed to both the pullback straps and the DAS umbilical cable. Two green pullback straps were required to lift the airplane up to the drop height, and stayed attached to the airplane after release, through the swing and impact. The straps attached to the airplane at the landing gear and over wing support, and were visible at impact as objects obstructing the pattern along the side of the airplane. The DAS umbilical cable connected the onboard data system to the controller inside the LandIR control room. It was required for triggering and data download after the impact, and was fastened to the tail at multiple locations to prevent motion of the cable during and after the impact event. It effectively divided the tail dot pattern into an upper and a lower portion.

Without the knowledge of the presence of the umbilical cable and pullback strap locations along with their expected motion during the impact, the data would show (falsely) large amounts of strain in the forward tail region due to the perceived large motion of the dot pattern at these locations from the movements of the cable and/or straps. Reporting the data around these areas would be in error. Figure 25, top, shows a close-up view of the straps and cable, along with the perceived strain computed at areas around these locations on the bottom.

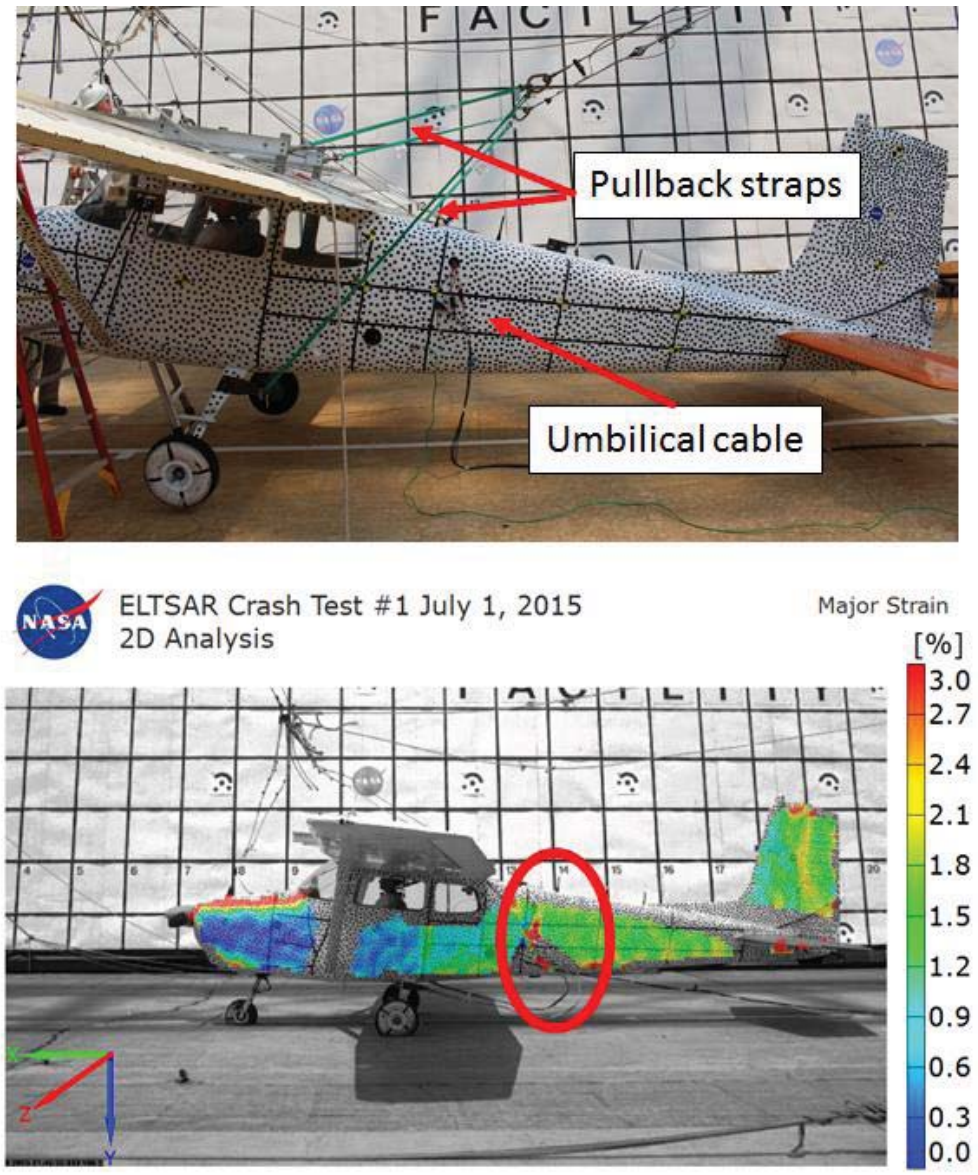

Figure 25 - Data analysis issues from ELTSAR tests

Figure 25, bottom, also shows additional data which require further examination before a full set of results can be presented. Note that the digital image correlation software defines the non-directional principle strain (ε_1) as major strain, which are calculated identically and mathematically equivalent. The "major" (and "minor" - which corresponds to ε_2) nomenclature will be used to report the non-directional principle strains ε_1, and ε_2. There is an area of high strain on the top of the engine compartment, and a small area of high strain on the bottom of the engine compartment, in front of the nose wheel. It first must be determined whether the strain shown is due to a real deformation from the test or due to errors in computation. Internal computations typically employ a smoothing algorithm where the surrounding points around an area in investigation get averaged into the computations. Many times, at edges where there are no surrounding

points to compute, the strain appears to be higher because the lack of additional data cannot be included in the smoothing algorithms. Thus, it must be determined whether the strain at an edge falls into this category or not. This process involves visual inspections of what is physically occurring at these edges (if possible), whether there is a perceived discontinuity from the software (i.e. the software tries to include background portions of the image unrelated to the object under investigation into the computational results) and/or the examination of the development in the time history of the strain. In most cases after using the described techniques, the strain at these edges is either removed from the data set or ignored.

There is also an area of high strain on the top of the vertical stabilizer. This high strain area is due to the computation error of strains at an edge. Finally there is a small portion of high strain right beneath the horizontal stabilizers in the tail. These data are clearly spurious, since it appears that the flexure in horizontal stabilizer, when viewed from the normal direction, is causing distortions in the dot pattern. These data will be ignored when conducting the final analysis of the airframe. With all of the above mentioned issues taken into account, the data from the ELTSAR test series were examined.

ELTSAR Test 1

ELTSAR Test 1 occurred on July 1, 2015. It represented an emergency landing with a high sink rate onto a rigid surface. The airplane impacted the surface at almost a level attitude, after which the main landing gear deformed outward until the tail came into contact with the rigid surface. The airplane rebounded from the surface with a large amount of horizontal residual velocity and impacted a yellow catch net which finally stopped the airplane horizontal motion. The 2-D and 3-D photogrammetric cameras were focused mainly on the initial ground impact location, with other cameras focused on the surrounding net area for post-impact response. Data generated from the other cameras were used for qualitative purposes only.

Impact conditions were first examined. Similar but smaller 3-in. diameter bowtie stickers were applied to notable areas on the skin of the airplane, as shown in Figure 26. Target locations chosen were the Engine, CG, Aft Cabin area, Station 142 (ST142), and Station 172 (ST172) in the tail. The impact velocity was measured at the CG of the airplane and angles were measured between the CG and the other dots. Because there was a pitch rate due to the test constraints, the angle (and angular rate) analyses were critical in determining the full characterization of the impact.

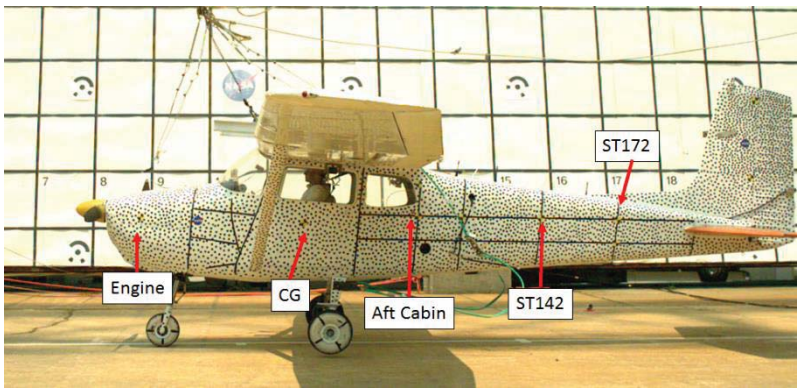

Figure 26 - ELTSAR Test 1 tracked target locations

Stickers were also placed on the Tail; however, the field of view of the 2-D tracking camera was not wide enough to resolve the location of the tail sticker prior to impact. This sticker was tracked after impact, and

the data exists if needed, however for the purposes of impact condition determination, this target was not used. The results for the horizontal and vertical velocities obtained from the tracking stickers are shown in Figure 27.

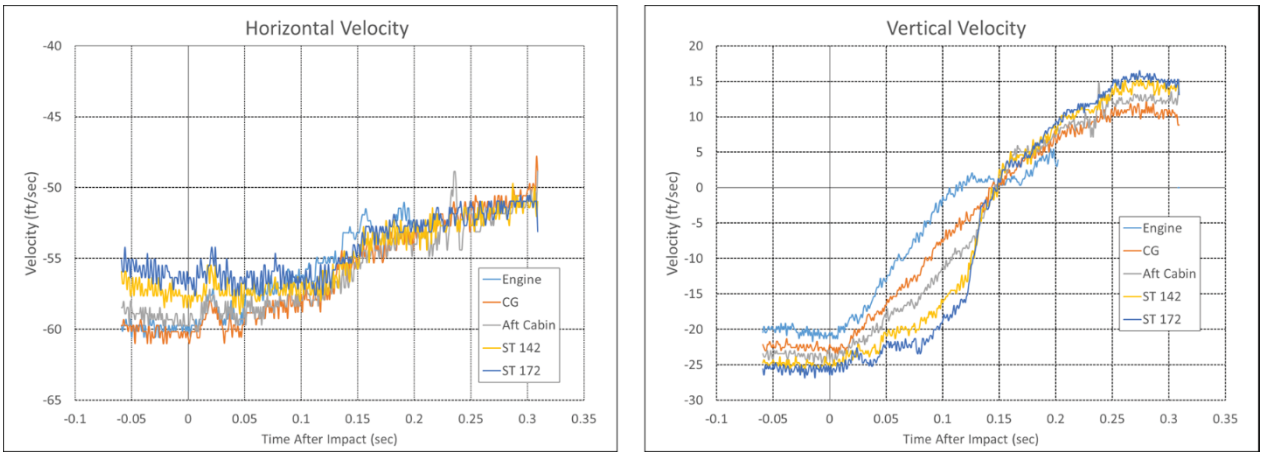

Figure 27 - ELTSAR Test 1 impact velocities

In Figure 27, data were able to be tracked approximately 0.050 sec. before impact and 0.300 sec. after impact. This duration is much shorter than the data that were able to be generated from the TRACT tests, due mainly to the higher velocity of the airplane at impact, which caused less camera frames to be available for use in tracking.

Further examination of the plots shows the traces both for the horizontal and vertical velocities were not identical at t=0.000 sec., suggesting that the 2-D impact condition tracking was able to capture the test article rotation prior to impact due to the pendulum swing. At 0.300 sec. after impact, the airplane still retained 88% of its original horizontal velocity at impact, indicating the airplane would have experienced a long roll out after the crash, and in a real landing, could have potentially hit an obstacle near the landing location. This scenario was anticipated, and in this test the airplane was stopped by a large yellow catch net, described above. In the vertical direction, the front of the airplane had the least amount of vertical velocity, while the rear part of the airplane had the most, indicating a positive pitch rate was present. The vertical velocity of the CG at impact was 23.0 ft./sec. The airplane vertical velocity reached zero approximately 0.150 sec. after impact, and the slow track back toward zero velocity was mainly due to the landing gear compression. After this time, the velocity changed direction, indicating a rebound. The rebound velocity reached a peak of between 10 and 15 ft./sec. at 0.275 sec. after impact, after which it moved out from the camera's field of view. Pitch angle was next examined and is shown in Figure 28.

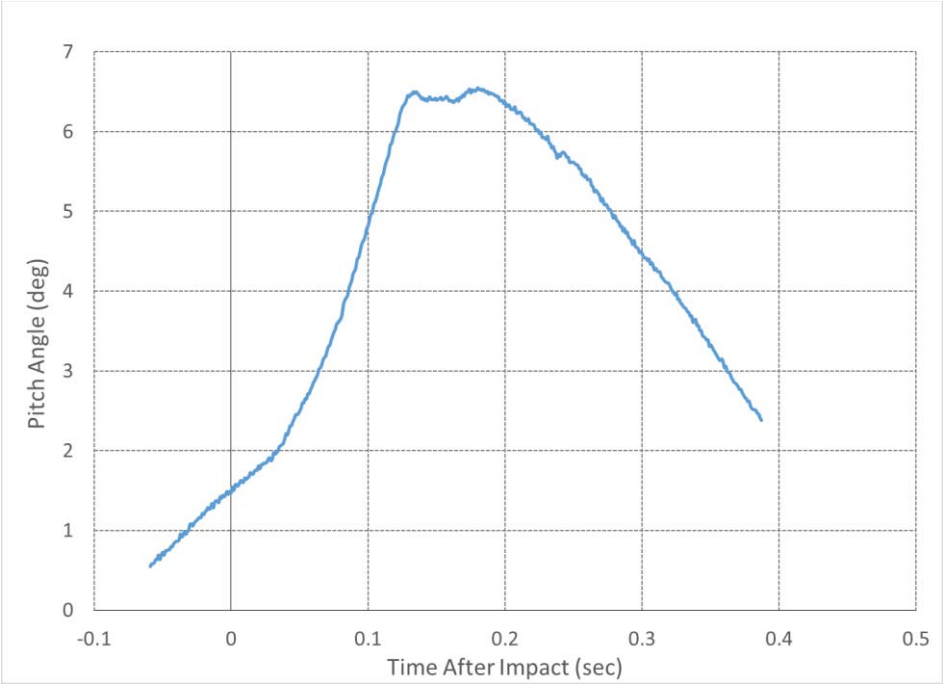

Figure 28 - ELTSAR Test 1 pitch angle

The pitch angle was found from the tracking software by tracking the horizontal angle between the CG and Engine targets throughout the impact event. Tracking starts at 0.054 sec. before impact and lasts through 0.387 sec. after impact. The first portion of the curve ranging between -0.054 sec. and + 0.03 sec. is linear. Taking the slope of this portion of the curve gives a rate of +16.5 deg./sec., indicating a rate causing the nose to pitch up. This rate is produced in the airplane due to the swinging via a single swing cabling system, and it is this rate which causes the velocities to not be identical at impact. The impact angle is 1.5 degrees, but the angle increases until it reaches a maximum of 6.5 degrees at 0.134 sec. after impact and retains this maximum value until 0.180 sec. after impact. It is during this time that the airplane crosses the zero vertical velocity mark and starts rebounding. After 0.180 sec., it starts heading back toward a level, 0 degree pitch condition.

Combining all of the impact tracking data produces a complete picture of the impact event. The airplane entered the field of view increasing vertical and horizontal velocity with a 16.5 deg./sec. pitch rate. The CG impacted at 60.2 ft./sec. horizontal and 23.0 ft./sec. vertical velocities at a pitch attitude of 1.5 degrees. Upon impact, the vertical velocity was reduced due to the landing gear compressing and the gear fully compressed approximately 0.150 sec. after impact. This compression pitched the airplane to a further positive angle until a maximum pitch angle of 6.5 degrees was reached. The airplane rebounded with a large amount of residual horizontal velocity and minimal horizontal velocity loss occurred for the next 0.150 sec. After 0.300 sec., the airplane passed out of the camera field of view.

The target-tracking analysis gave insight into the response of the airplane during the impact event. However, the digital image correlation results will next be examined to investigate airframe response further. After removing all perceived spurious data, there were only small portions of the airframe which gave data usable for analysis, shown in Figure 29. The four major areas where data were resolved on the

airplane were the engine compartment, the cabin, the mid-to-rear tail and the vertical stabilizer. The dot spacing used on the airplane gave a data point every 1.75 in. along the skin of the airplane.

Figure 29 - Data set resolved for use in ELTSAR Test 1 analysis

The non-directional result of major strain was first examined. Figure 30 shows the major strains present at 0.052 sec. after initial impact.

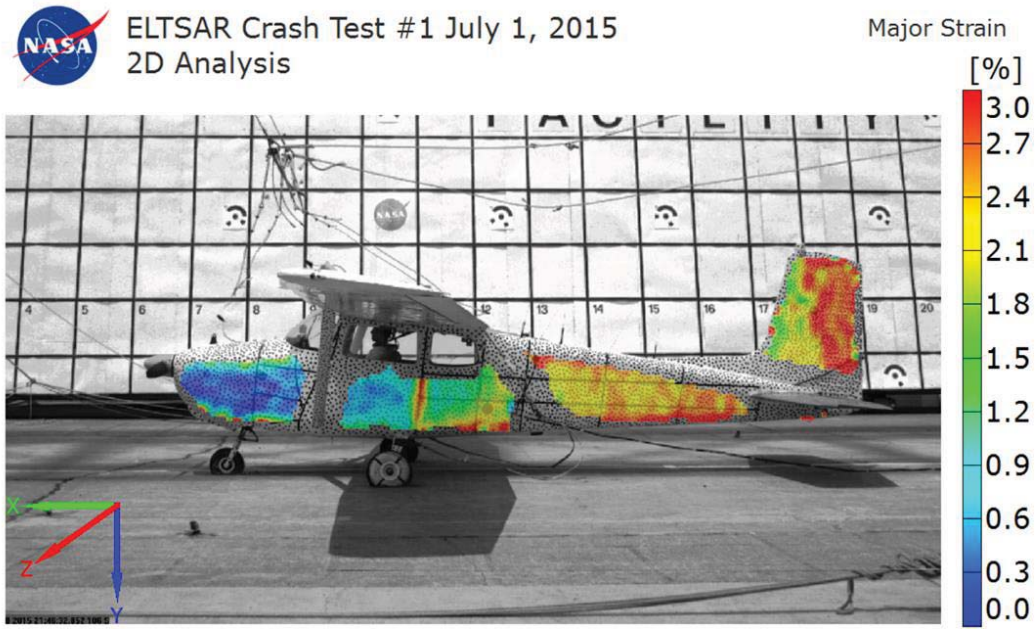

Figure 30 - Major strain at 0.052 sec. in ELTSAR Test 1

The fringe plot of major strain gives a good insight to where the large amounts of positive (tensile) strain are occurring at a specific time. The major items to note are the areas on the vertical stabilizer where almost 3% strain is occurring and on the Mid Tail section, which showed almost 2% strain. There is also a line of high strain between areas of low strain where the door closes in the cabin. The area on the tail which shows high strain does not affect the rest of the airframe response, so it will not be investigated further. The non-directional result of minor strain was next examined. Minor strain data are a quick way of determining areas under high compressive loading on the airframe. Figure 31 shows the minor strain present 0.052 sec. after initial impact, which is the time after impact in which the main landing gear were halfway deflected.

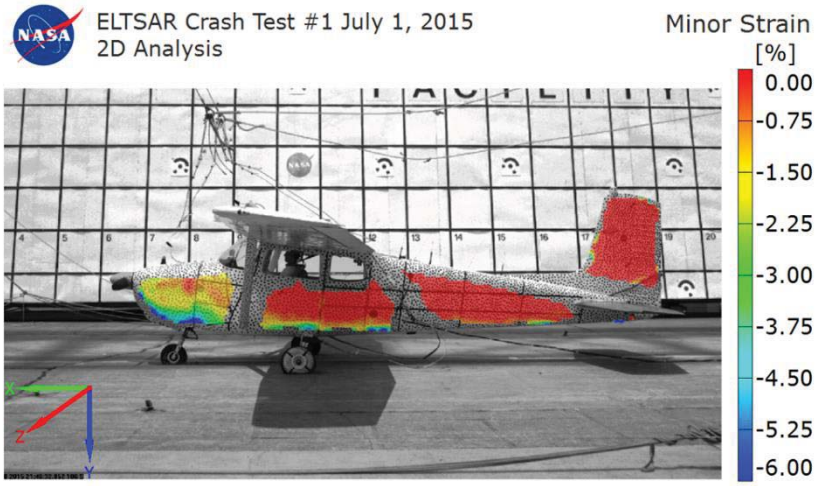

Figure 31 - Minor Strain in ELTSAR Test 1

Not unexpectedly, areas of large minor strain occurred mainly on the bottom of the airframe, at areas near the landing gear attachments. The largest minor strain occurred on the skin at the nose gear attachment. The compressive strain was examined by plotting the vertical (Y) strain, and values from particular areas on the airframe were extracted. Figure 32 shows the vertical strain, along with the locations for the extracted values.

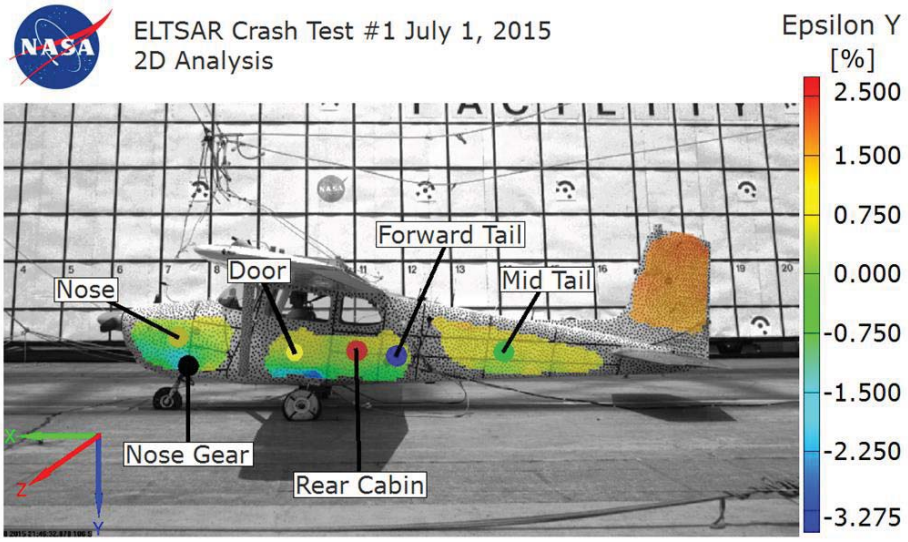

Figure 32 – Vertical (Y) strain in ELTSAR Test 1

Large negative strains appeared around the landing gear locations, indicating compressive vertical loading at these areas, which follow the trends first shown in the minor strain plot in Figure 31. However, negative vertical strains were localized to the areas immediately adjacent to the landing gears. The negative values were expected due to the gear compression. The tail, in contrast, showed positive strain which was due to the tension caused in the tail from flexure. The vertical stabilizer also showed large positive strain. Time histories of the vertical strain at various locations on the airplane are shown in Figure 33.

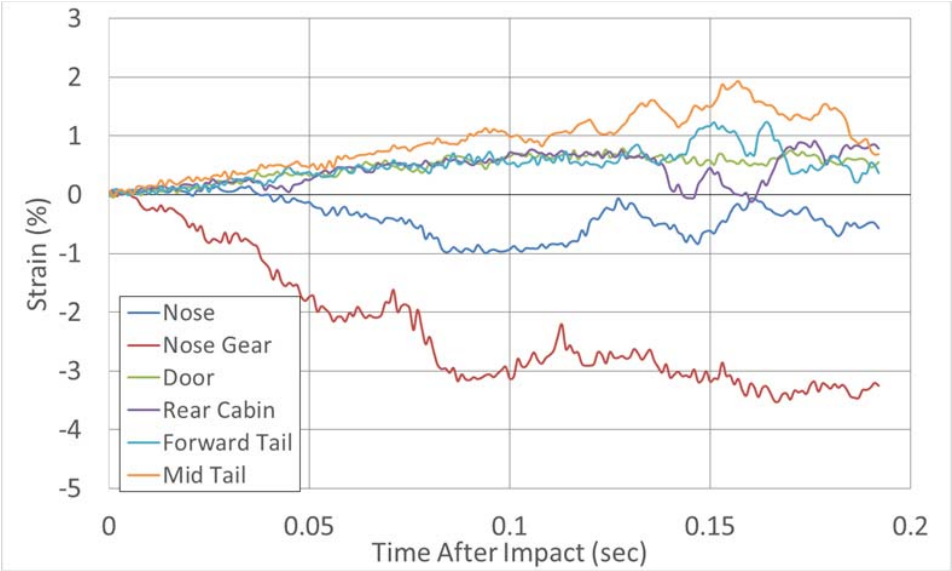

Figure 33 - Vertical (Y) strain time histories from ELTSAR Test 1

The area immediately adjacent to the nose gear experienced the most compression, which leveled off at approximately 3.5% compressive strain at just before 0.200 sec. after impact. At the 0.200 sec. time, the airplane started to rebound and some of this strain would have potentially dissipated, and the permanent strain due to the impact could have been determined. However, because the camera field of view did not capture the entire rebound, no further analyses was completed. Figure 33 also shows that the only other negative strain occurred on the skin of the nose. While Figure 32 shows negative strain around the main gear locations, this strain has dissipated when examining the strains on the door, which are slightly positive. The Mid Tail strains are the most positive, which shows almost 2% positive strain in tension due to the tail flexure.

ELTSAR Test 2

Test 2 was conducted on July 29, 2015, and represented a CFIT impact scenario. The airplane impacted in a nose down condition onto the soil, which stopped its forward velocity almost immediately. The nose stuck into the soil, stopped, and caused a pivot point about which the rest of the airplane rotated. The airplane rotated about the nose, flipped over and came to rest upside down near the original impact location. The impact sequence can be seen in Figure 24. Similar to Test 1, impact conditions were first examined. Bowtie stickers were placed in the same locations as used on Test 1, and similar points were tracked throughout the crash sequence. The impact velocity was measured at the CG of the airplane and angles were measured between the CG and the other dots. Figure 34 shows the dot locations while Figure 35 shows the time histories of the dot positions throughout the crash sequence. The view was changed slightly to accommodate a target on the vertical stabilizer, which, unlike ELTSAR Test 1, was able to be tracked prior to initial impact.

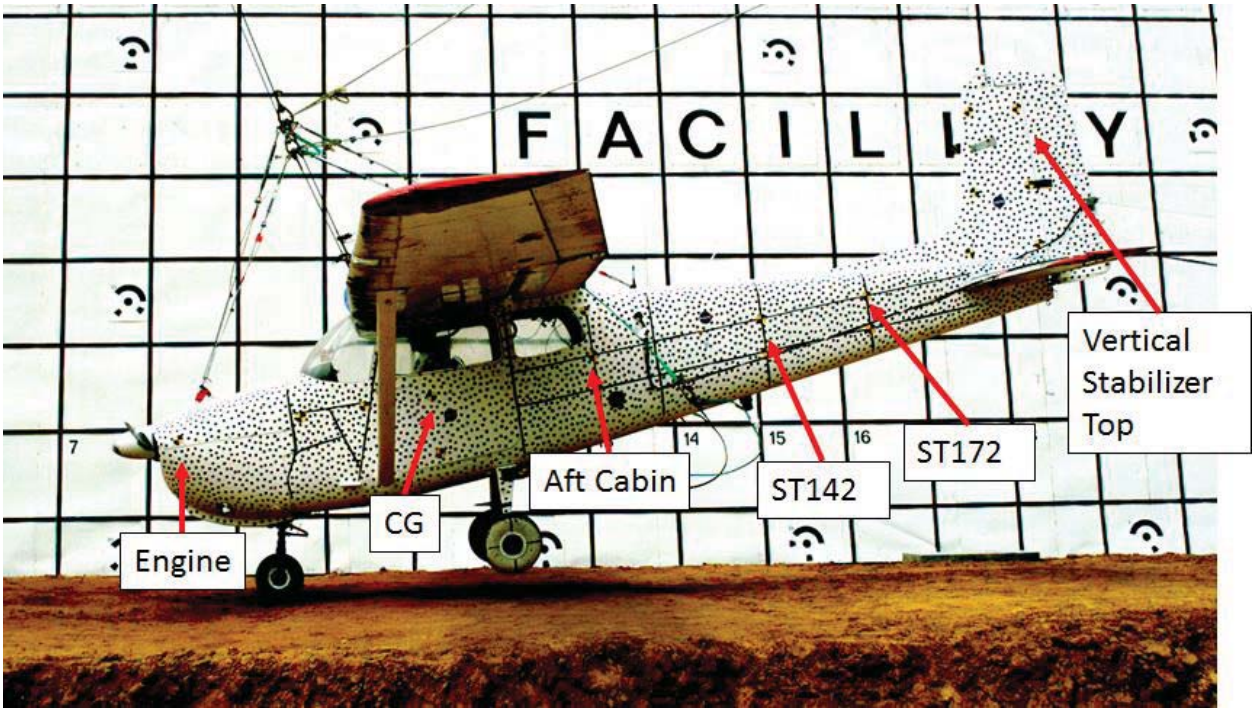

Figure 34 - ELTSAR Test 2 tracked target locations

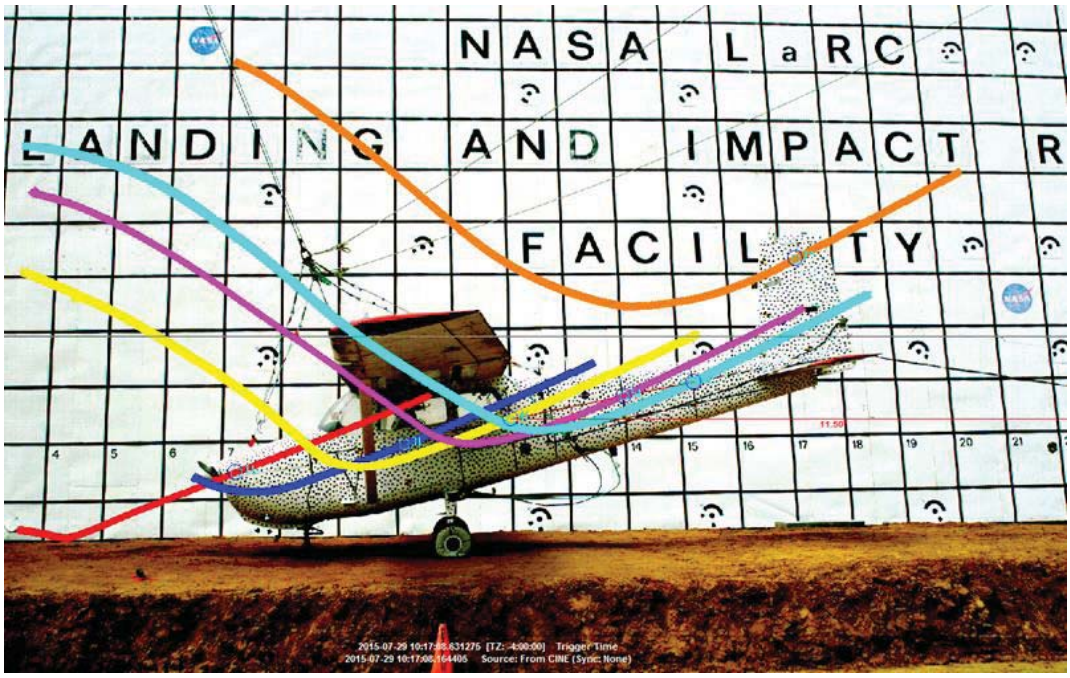

Figure 35 – ELTSAR Test 2 target tracking marker time history

A qualitative view of the graphical representation of the tracked targets in Figure 35 reveals information about the impact and immediate post-impact response. The tracked time history of the targets shows a remarkable difference in displacement between the targets in the front of the airplane to those on the rear of the airplane. For example, the nose, in red, shows a straight line movement of forward and downward motion until the surface is impacted with a very small rebound. The target on the tail, in orange, however shows forward and downward motion until the displacement reaches a minimum, changes direction and then begins to exhibit a large upward motion. Other targets on and near the tail of the airplane show similar responses. These results are actually showing the rotation of the aircraft around the nose, which acts as the pivot point. The targets do a good job of tracking the airplane rotation making it easy to quantify using created angle measurements.

The targets were next used for impact velocity calculations, which are shown in Figure 36. The airplane arrives in the camera field of view 0.070 sec. before impact, and the camera is able to track most of the targets past 0.500 sec. after impact. The engine and CG targets get obscured from the extreme amounts of deformation due to the ground impact and are only able to be tracked for the first 0.200 sec. after impact. Using the data in Figure 36, the impact conditions at the CG were 68.6 ft./sec. horizontal velocity and 28.7 ft./sec. vertical velocity. As with Test 1, the velocities at all points at the time of impact were not identical due to the pitch rate of the airplane during the swing.

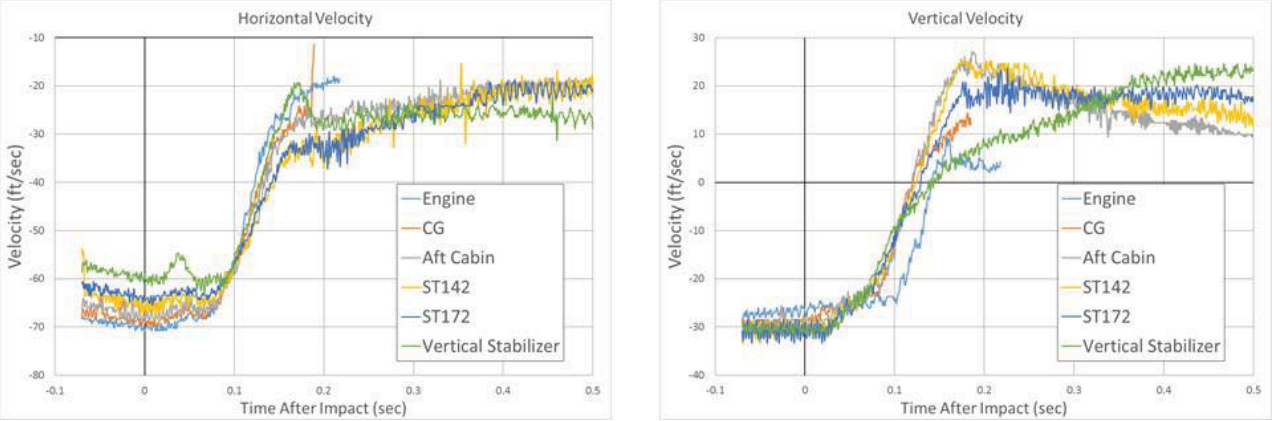

Figure 36 - ELTSAR Test 2 impact velocities

As shown in Figure 37, the angle of the impact was computed using the tracked points identified in Figure 34. As with the velocity points, the angle was able to be measured both before impact, resulting in an angular rate impact condition, along with almost 0.700 sec. after impact, showing the post-impact response. The points used in the angle analysis were located on the tail, since the points in the front of the cabin and nose were unable to be tracked approximately 0.200 sec. after impact due to the large deformation of the nose and forward cabin.

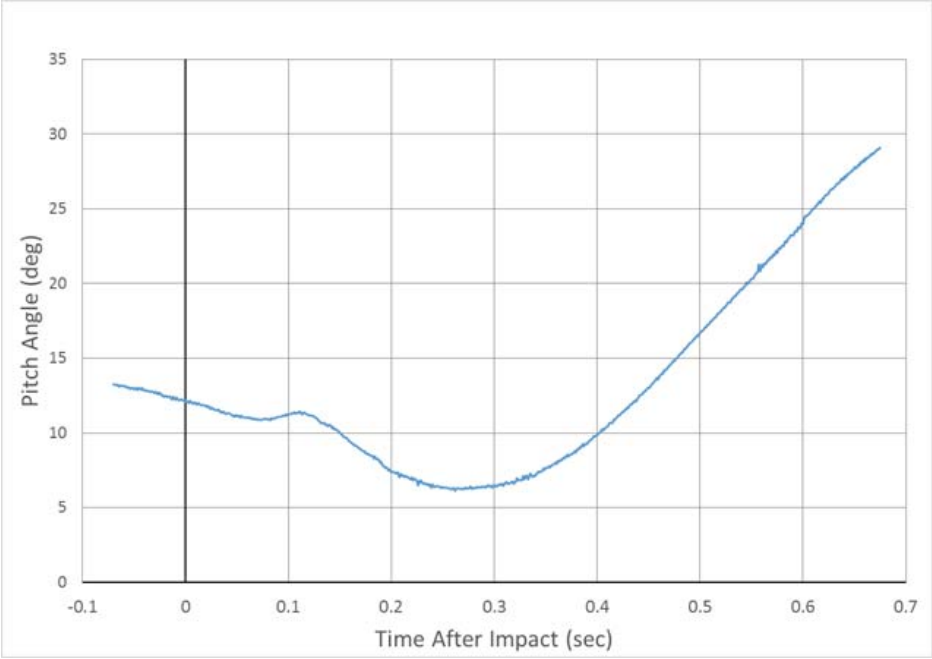

Figure 37 - ELTSAR Test 2 pitch angle computation

By computing the slope of the angle prior to impact, the pitch rate at impact was found. The pitch rate, by using the slope, was computed to be +16.1 deg./sec., and taking the intersection of the pitch data at impact gave a pitch angle of 12.2 degrees nose down. The tail angle began trending with a positive slope approximately 0.080 sec. after impact, however the angle starts to trend back toward zero due to the initiation of the tail buckling which offset the airplane rotation. The angle immediately begins increasing

again at approximately 0.270 sec. after impact, which was after the tail buckle has reached a maximum, and the rotation of the airplane has begun to take over the major angle change effect. Inspection of the slope of the line after 0.400 sec. after impact resulted in a rotation rate of 72.5 deg./sec. during the airplane rotation.

There was a substantial amount of damage on the airframe due to plowing and rotation. The strain on the skin was next examined in an attempt to quantify the deformation. Figure 38 presents major strain on the airframe approximately 0.021 sec. after initial nose gear to soil contact.

Figure 38 - ELTSAR Test 2 major strain at t+0.021 sec

Figure 38 also shows the erroneous data on the tail at the location of the DAS umbilical, which was also seen in ELTSAR Test 1. After ignoring these data, the major result is shown on the nose at the firewall location. The nose wheel has started to penetrate the soil, which creates a pivot point for the start of rotation. The strain developed at this location is the beginning of the deformation of the nose of the aircraft due to the rotation about the nose wheel, while the majority of the rest of the airframe is unaffected at this time. Figure 39 shows the major strain developed a short time later, at 0.063 sec. after impact, or 0.042 sec. after the data shown in Figure 38.

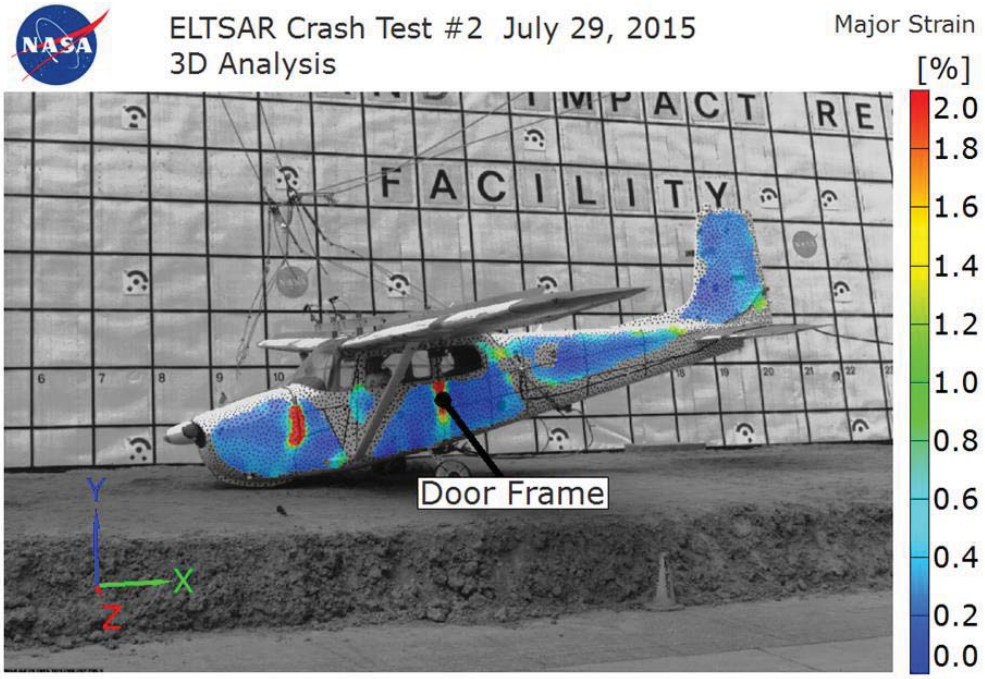

Figure 39 - ELTSAR Test 2 major strain at t+0.063 sec

Figure 39 shows that the nose wheel has now penetrated fully into the soil, developing very large major strain at the firewall location on the nose. It also shows large amounts of major strain developing at the door opening location in the cabin of the airplane. This location is where the door latches into the body of the airframe, and, as shown in Test 1, represents a discontinuity in the airframe skin. It is easy to see why the strain would develop here as the relative motion between the door frame and airframe body would show up as a perceived strain in the data, which is really a weak spot in the airframe. A point in this high area of strain at the door frame location was picked for further interrogation, and the time history is shown in Figure 40.

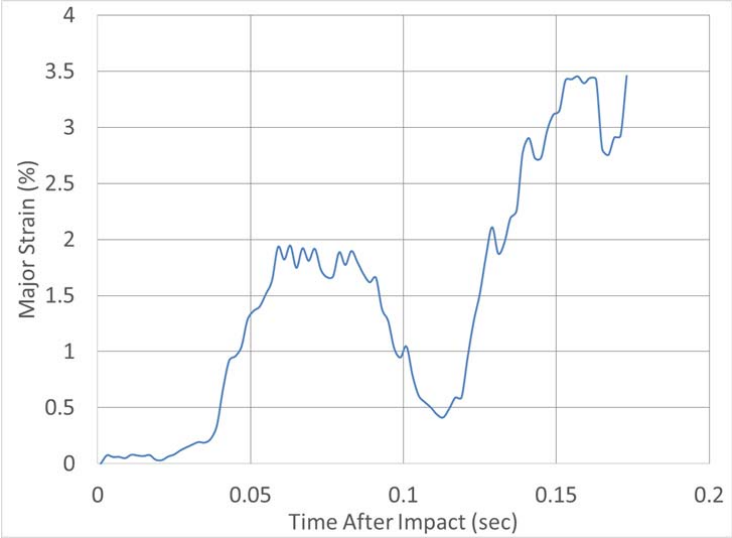

Figure 40 - ELTSAR test 2 door frame strain time history

The strain plotted in Figure 40 reaches an initial peak of 1.9% approximately 0.059 sec. after impact and plateaus for the next 0.024 sec. It then dips down to a minimum of 0.41% at 0.113 sec. after impact. It returns to almost 3.5% at 0.155 sec. after impact and stays at this value until the data are unable to be tracked further. The initial plateau and then minimum suggests a stress wave traveling through the airframe skin due to the initial impact at the nose. The strain reaches a minimum after the wave has passed, but then heads back to a permanent value of almost 3.5% when the airplane finally starts to flip over, suggesting that the flipping permanently deforms the airframe. Shortly after 0.150 sec., the extreme deformation of the aircraft obscures the majority of the dot pattern on the engine and cabin so tracking near the front of the airplane is not possible. However, the portion of the tail aft of the buckling deformation is a portion of the aircraft which is able to be tracked for the next 0.700 sec. Figure 41 shows a fringe plot, along with a time history of major strain on the portion of the tail capable of being tracked.

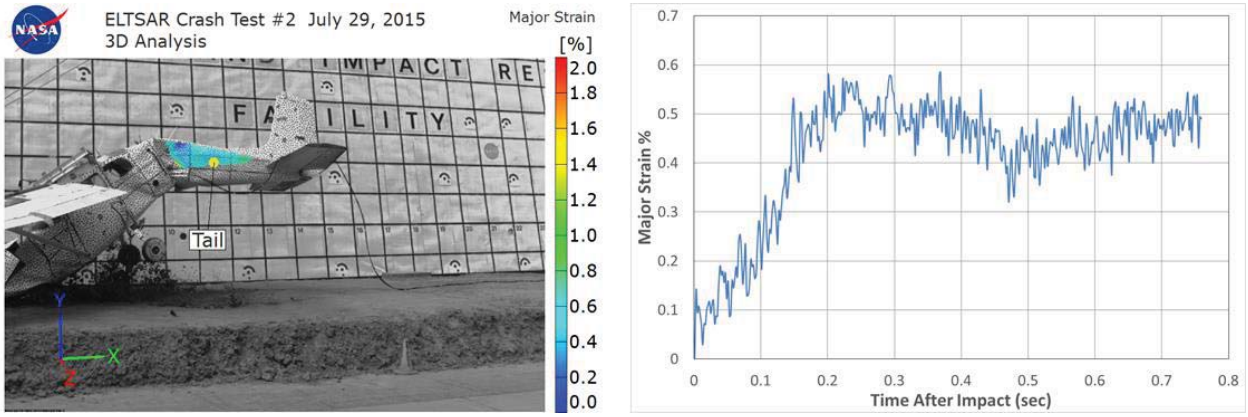

Figure 41 - ELTSAR Test 2 major strain on tail.

The deformation on the tail was able to be tracked late into the time history of the crash. It is important to note that the tail reached a maximum of almost 0.6% and sustained major strain of between 0.4 and 0.5%, which occurs 0.200 sec. after impact. Much like what was seen in the door frame data, it is at this time when the strain seen in the door also reaches its maximum sustained strain value due to the flipping of the airframe.

ELTSAR Test 3

Test 3 was conducted on August 26, 2015. The test represented a CFIT impact scenario, in which the pilot senses an impact is imminent, and unsuccessfully attempts to pull the nose of the airplane up, resulting in a tail strike scenario. The test resulted in the airplane impacting the surface nose up, and tail down. The tail impacted the surface, which caused a rotation about the tail, resulting in a "slap down" effect in the nose, much like what was seen in the TRACT tests. The nose and nose gear proceeded to dig into the surface, which then caused a rotation about the nose, resulting in the airplane flipping over and landing upside down, much like what was seen in ELTSAR Test 2. At a point in the rotation from flipping, a large portion of the tail failed at the cabin-to-tail transition area, leaving only a small portion of the skin to retain the tail onto the rest of the airplane. Unlike ELTSAR Tests 1 and 2, the 2-D impact condition tracking camera did not trigger correctly. The impact conditions, consequently, were found using a combination of the cameras utilized for the 3-D digital image correlation analysis and the real-time high-definition cameras. Impact velocities were found by using the 3-D deformation cameras and creating points nearest to the target

sticker locations as possible using the full-field grid. Impact angle was found using a 2-D analysis of the airplane orientation at the frame of impact. It was important that there were redundant cameras filming the impact and post-impact response, as the impact conditions would not be able to have been found if these were not present. Figure 42 shows the created tracking markers, as obtained from the 3-D deformation analysis.

Figure 42 - ELTSAR Test 3 tracked target locations

All of the bowtie markers used specifically for the 2-D impact condition analysis on the airplane were not able to be tracked with the 3-D deformation cameras due to data limitations outlined in the *Data Interpretation Limitations* section. The wing strut obstructed the view of the CG sticker, and therefore, the CG was tracked via the NASA logo sticker, which was applied approximately 6 in. below the CG sticker on the door. The two other locations used for the determination of impact velocities and attitudes were located on the front and rear of the airplane. In the front, the sticker on the nose near the firewall and battery cover was used. In the rear, the position near the sticker at the ST172 location was used. However, because the point picked was not at the exact ST172 location, it was generically called "Tail." Figure 43 shows the time history of the three tracked points.

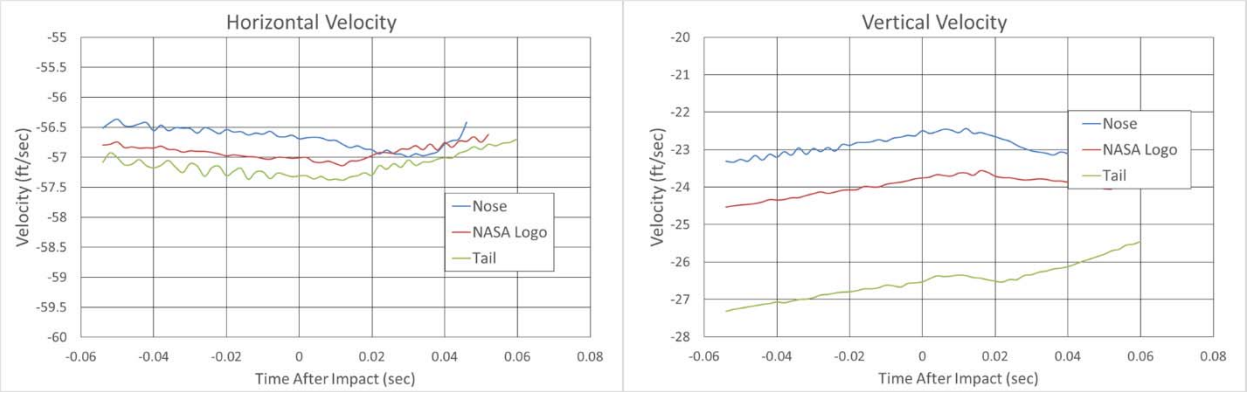

Figure 43 - ELTSAR Test 3 impact velocities

As with the first two ELTSAR tests, the velocities at impact are not identical due to the rotation of the test article from the swing prior to impact. The configuration of the cameras used for the 3-D analysis did not allow for a large portion of the time history of the impact conditions to be tracked so the analysis occurred within 0.060 sec. before to 0.060 sec. after impact. Had the 2-D camera triggered, it would have obtained a large amount of time history data prior to and after the impact, much like what was seen in ELTSAR Tests 1 and 2. Further data analysis was not completed from the standpoint of the impact conditions.

To find pitch and pitch rate, angle analysis was performed from a single frame of high definition video from the camera positioned normal to the flight path. By measuring the angle between the tail and the horizontal lines on the backboard at impact, a total angle of 13.7 degrees was found. Subtracting the 5.7 degree natural inclination of the tail from the total angle resulted in a pitch angle at impact of 8.0 degrees. The pitch rate was found by reusing the points obtained from the 3-D deformation data. The angle itself was not used as the impact angle since the points were not created specifically to provide an angle measurement; however, by taking the slope of the angle vs. time plot, the rate of change of that angle with respect to time can be found. This rate of change is the same for all created angles on the aircraft while exhibiting rigid body motion during the swing, so the choice of where the angle is created did not matter. Figure 44 shows the pitch angle at impact using a still frame from the high-definition video, and a plot of the 3-D data in which the slope of the curve is the pitch rate.

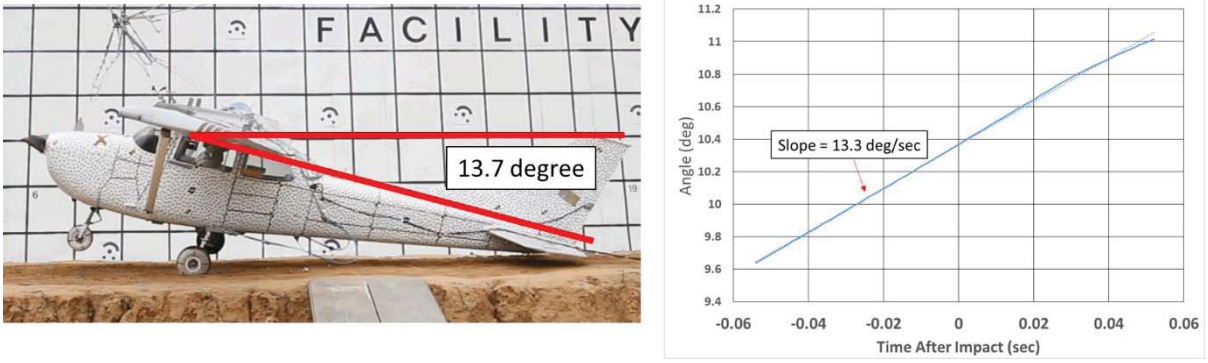

Figure 44 - ELTSAR Test 3 angle analysis

Further analysis of the pitch angle which occurred after the impact was not completed due to frame rate limitations from the real-time camera. The deformation of the airframe resulting from the impact was next examined from the 3-D deformation data. As with Tests 1 and 2, non-directional major strain was first examined to find areas of large deformations. Figure 45 shows the major strain on the airplane at 0.052 sec. after impact.

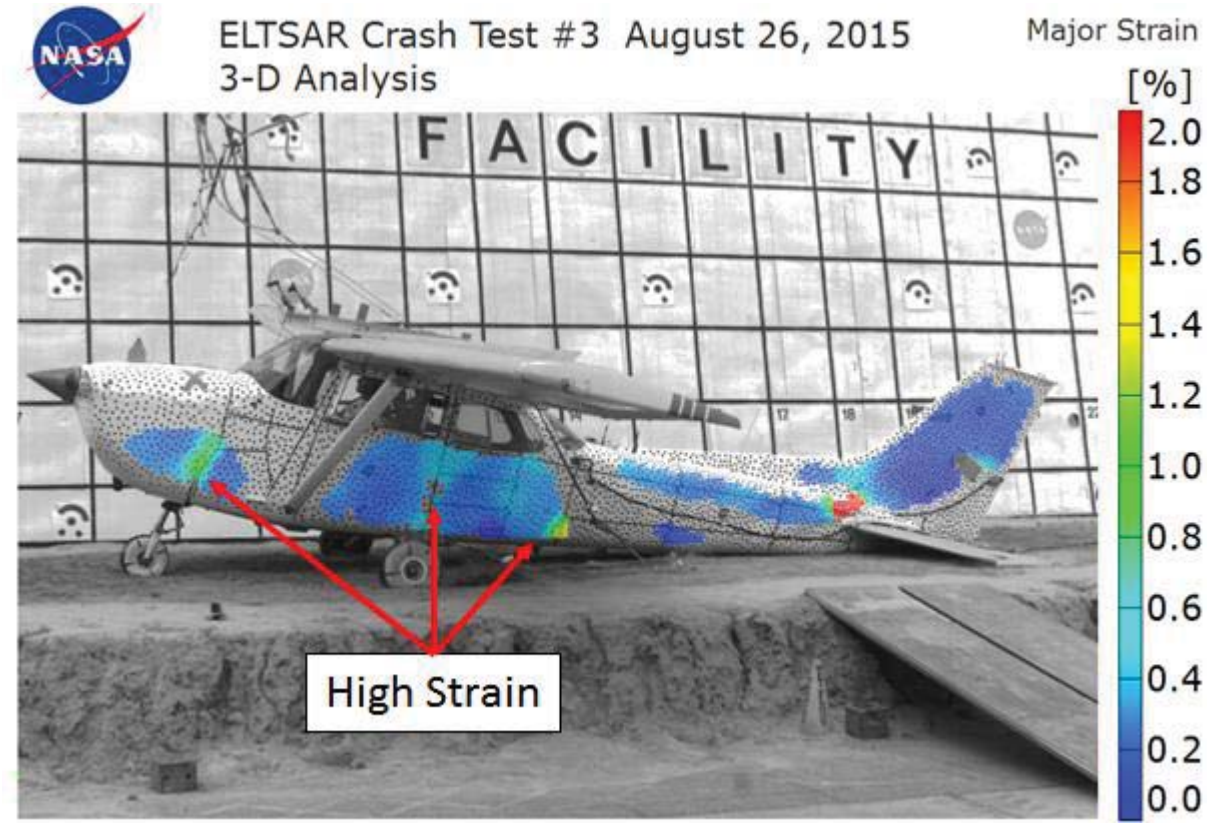

Figure 45 - ELTSAR Test 3 major strain at t+0.052 sec.

As with the previous tests, the area immediately surrounding the umbilical cable was not computed due to complications arising from the cable interference with the dot pattern. Even with this area not computed, spurious strain shows up in the data at the location where the horizontal stabilizer, vertical stabilizer and the DAS cable meet near the rear of the tail. The strains in this area were ignored due to the discontinuity at this location. As seen in the previous two tests, there were high strains at the nose gear, door location and rear cabin locations. Similarly to what was examined for ELTSAR Test 1, points along the side of the airplane were picked for further examination. Figure 46 shows the locations of the picked points.

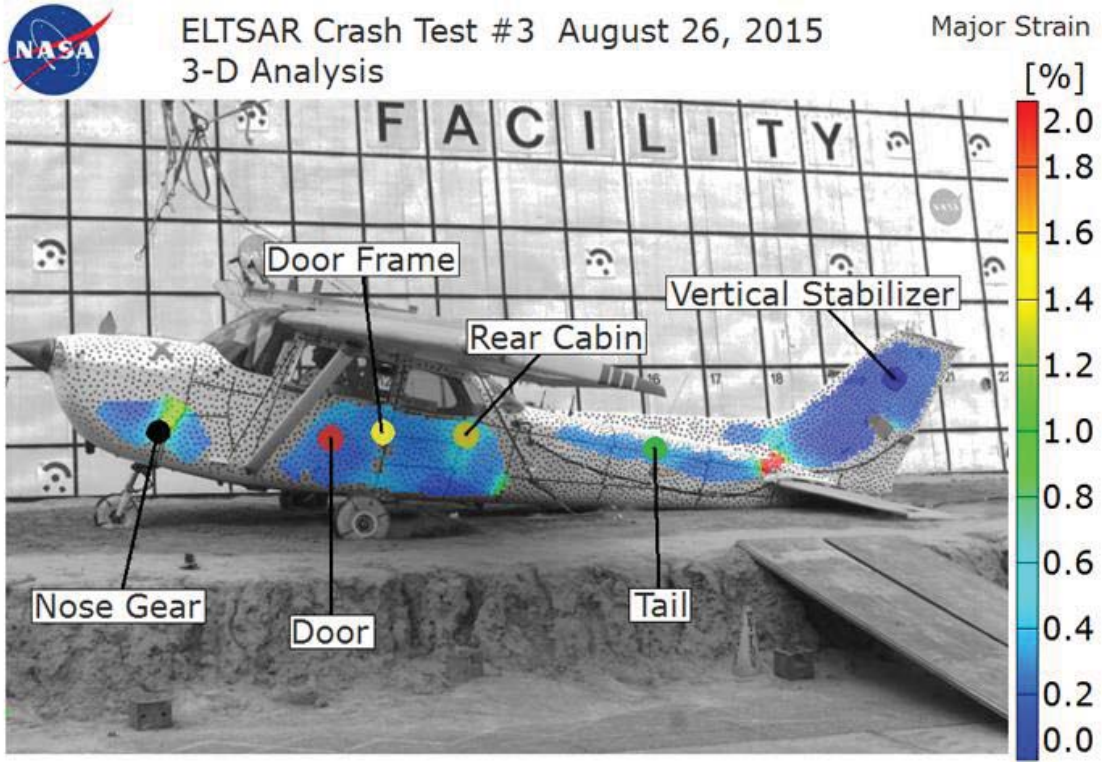

Figure 46 - ELTSR Test 3 point locations

The points were extracted from Figure 46 and their time histories were plotted. Figure 47 shows the time histories from the test.

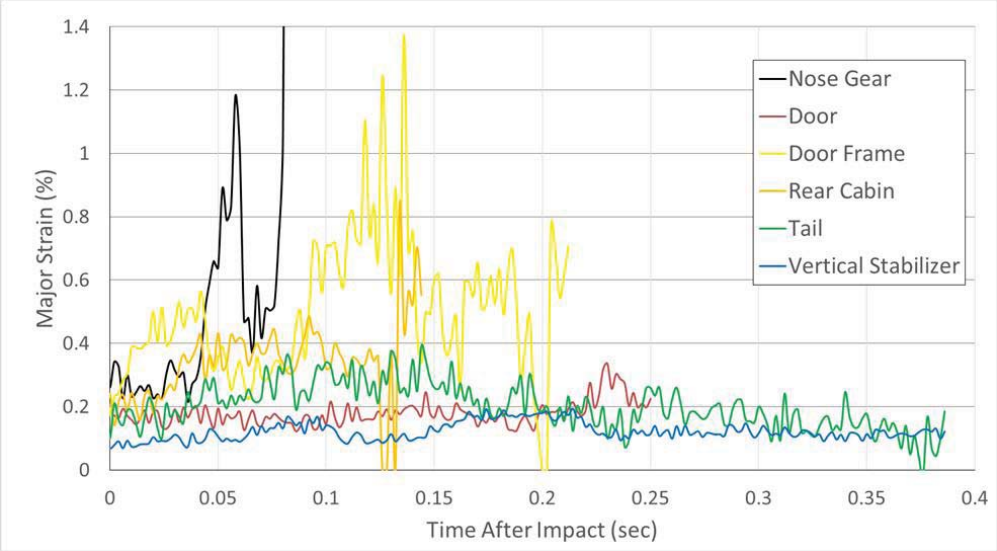

Figure 47 - ELTSAR Test 3 point major strain time histories

The data in Figure 47 shows high major strain mainly occurring in the nose gear, which peaks at 4.5% (not shown) at 0.084 sec. after impact. It is at this time where the maximum vertical displacement of the nose gear occurred, but before the airplane started to flip over. The high strain then moves to the door frame at approximately 0.125 sec. after impact, which is due to the airplane rotation. The high strain has moved from the nose, down the longitudinal axis of the airframe and impacted the cabin during this time. Similar to Tests 1 and 2, the door represented a discontinuity in the airframe skin and displayed high strains when compared to the surrounding airframe structure. Major strain data on the rear cabin also reached a peak sometime after 0.130 sec. after impact. It is near this location where the main structural failure occurred. The major strain in the tail reached a strain value of approximately 0.4% due to tail flexing before the failure, while the vertical stabilizer was largely unaffected from the crash. Its strain data reached peak values of below 0.2% strain.

Discussion

A variety of photogrammetric techniques used in full-scale crash testing are presented in this report. These techniques include 2-D impact condition tracking, 2-D and 3-D full-field digital image correlation airframe deformation tracking, ATD motion tracking using applied targets, onboard airframe structural tracking and markerless ATD motion tracking. These techniques utilize the full range of measurement capabilities and equipment which include high definition, high-speed, onboard, off-board and markerless tracking types of cameras.

The determination of the impact conditions through the use of tracked dot positions on airframe is critical for post-test analysis. The impact conditions are needed to provide specifics of the impact, which are typically used to define the severity of crash scenarios. Additionally, if computer models are developed in conjunction with the crash testing - as they were in both of these test series - the precise conditions are needed so that valid simulation scenarios can be represented. The dot tracking 2-D impact analysis typically utilized a single high-speed camera oriented normal to the flight path of the vehicle which, in these cases was a 2 MP high-speed camera imaging at 1 kHz. The dot tracking using this configuration was successful in 4 of the 5 tests presented, while a triggering issue causing the camera to miss the coverage of one impact event. In that test, because redundant cameras were present, a combination of 3-D deformation tracking and real-time camera views were able to supplement for the missing coverage. This coverage, however, was not nearly as robust as the high-speed video coverage.

The 3-D digital image correlation was utilized for the first time at the LandIR facility for the TRACT 1 crash test. Previous to this test, it was unknown whether the technique was capable of working on such a large scale deformable test article undergoing a dynamic crash test. The TRACT 1 crash test featured black 1-in. dots on a white background over the entire left side of the aircraft. The 3-D deformation full field tracking utilized a pair of synchronized 4MP high-speed cameras imaging the immediate impact location at 500 Hz. The resultant deformation analysis proved highly successful and offered insight into the test article deformation during impact. The large amount of out-of-plane deformation which occurred along the side of the airframe was able to be measured quantitatively for the first time. The time history of this deformation, as capable of being measured from the 3-D deformation analysis, also showed that this deformation was elastic. The analysis also showed areas where permanent deformation was present.

Upon successful analysis from TRACT 1, the 3-D digital image correlation technique was used on all subsequent tests presented in this report. The technique was successful for TRACT 2 and ELTSAR Tests

2 and 3. Deformation data obtained from the TRACT 2 test article showed that the airframe experienced a significantly different deformation profile than for TRACT 1. The deformation data, along with the impact condition analysis, showed that the TRACT 2 test article exhibited significantly higher shear loading, which led to large amounts of permanent deformation, especially in the forward cabin section.

For ELTSAR Test 1, a 2-D version of the digital image correlation analysis was utilized. The 2-D analysis was used instead of 3-D analysis because the calibration for the 3-D deformation analysis was not able to be completed. ELTSAR Test 2 showed large strains at the firewall location at impact. It also showed large strains at the door opening, which is not unexpected due to the discontinuity in the aircraft skin caused by the presence of the door.

The ELTSAR tests show airframe strain due to three different crash test scenarios of Cessna 172 aircraft. Notable results showed the highest strains on the airframe occurred at the landing gear attachment locations and typically the lowest strains occurred far away from the impact at locations like the vertical stabilizer. High strain at the door locations was also present due to the discontinuity in the aircraft skin at these points, suggesting the weak point in the airframe is at the door frame location. The tail in all three tests exhibited a varying amount of flexing, and the vertical stabilizer seemed unaffected from the crashes in the three tests. Finally, the results presented only represent a small subset of the acquired results obtained from the full-field pattern. Now that the data are acquired, it is available and can be further interrogated when the need arises.

Sample uses of onboard high-speed cameras are also presented in this report. First available for use in the TRACT 1 test, ruggedized high-speed cameras capable of being utilized onboard during the crash tests offer insight into phenomena occurring onboard not able to be definitely measured through the instrumentation alone such as accelerometers, strain gages or load cells. In TRACT 2, specifically in the subfloor region, an onboard camera provided a definitive way of tracking airframe deformation previously unavailable.

This report also highlights the need for a redundant setup when attempting to acquire all of the various types of data described above. During ELTSAR Test 3, at least one or more of the cameras did not trigger, and missed the impact event. Because there were multiple cameras and multiple ways of conducting the analysis, all of the required measurements were successfully obtained. Typically, for a given crash test, there are 15 high-speed and 4 to 10 real time ground cameras, representing a wide range of redundant coverage options available. However, there is no redundancy built into the onboard cameras at the current time. Fortunately, an onboard camera has yet to fail for all tests conducted thus far. Consideration will be given to redundant onboard cameras should the need and application arise.

It is important to note that the data plots, time histories and pictures presented in this report were created exclusively through the utilization and manipulation of camera images. While remarkable, the obtained data must be used in conjunction with other sensor data to gain a complete picture as to the sequence of events and failures which occur.

Finally, this report presents the current capabilities and typical imaging techniques in use at the LandIR facility. However, new techniques are always in development, data processing algorithms are always being written, and equipment is always improving. As cameras get smaller, they can be placed in previously inaccessible areas furthering the quantitative data collection analysis areas. As cameras get less expensive,

many more can be used in testing, which will offer redundant coverage when critical applications need it. Finally, as computers get faster, their processing power will be able to match the improvement in camera resolution, and hopefully provide even further detailed coverage of the initiation and propagation of the various types of failures seen in the results provided. It is anticipated that the state-of-the-art keeps advancing as tests are conducted at the LandIR facility, and the data generated can ultimately be used to design and analyze better aircraft.

Acknowledgements

The author would like to acknowledge NASA's Revolutionary Vertical Lift Technology (RVLT) Program (formerly Rotary Wing Program) for its support of the full-scale TRACT tests, with the support for allowing experimental techniques and equipment to be placed onboard. The author would also like to thank the Search and Rescue (SAR) Mission Office at NASA's Goddard Space Flight Center for allowing the author to paint three Cessna 172 aircraft for the acquisition of photogrammetric data. The photogrammetric results will hopefully reinforce the SAR Mission Statement and ultimately save lives.

References

1. Vaughan, V.L. and Alfaro-Bou, E. "Impact Dynamics Research facility for Full-Scale Aircraft Crash Testing." NASA TN-8179. April 1976.

2. Jackson, K.E., Boitnott, R.L., Fasanella, E.L., Jones, L.E. and Lyle, K.H. "A History of Full-Scale Aircraft and Rotorcraft Crash Testing and Simulation at NASA Langley Research Center." NASA TM-2004-0191337. January 2004.

3. Littell, J.D. "Full-Scale Crash Test of an MD-500 Helicopter." Proceedings from the American Helicopter Society Forum 67. Virginia Beach VA. May 3-5, 2011.

4. Jackson, K.E., Littell, J.D., Horta, L.G, Annett, M.S., Fasanella, E.L. and Seal, M.D. "Impact Testing and Simulation of Composite Airframe Structures." NASA TM-2014-218169. February 2014.

5. Annett, M.S., Littell, J.D., Jackson, K.E., Bark, L.W., DeWeese, R.L. and McEntire, B.J. "Evaluation of the First Transport Rotorcraft Airframe Crash Testbed (TRACT 1) Full-Scale Crash Test." NASA TM-2014-218543. October 2014.

6. Annett, M.S. and Littell, J.D. "Evaluation of the Second Transport Rotorcraft Crash Testbed (TRACT 2) Full Scale Crash Test." Proceedings from the American Helicopter Society 71st Annual Forum. May 5-7, 2015. Virginia Beach Virginia.

7. Littell J.D. "Crash Tests of Three Cessna 172 Aircraft at NASA Langley Research Center's Landing and Impact Research Facility." NASA TM-2015-218987. November 2015.

8. Melis M.E., Brand, J.H., Pereira, J.M. and Revilock, D.M. "Reinforced Carbon-Carbon Subcomponent Flat Plate Impact Testing for Space Shuttle Orbiter Return to Flight." NASA TM-2007-214384. 2007.

9. Hilburger, M.W., Waters, W.A. and Haynie, W.T. "Buckling Test Results from the 8-Foot-Diameter Orthogrid-Stiffened Cylinder Test Article TA01." NASA TP-2015-218785. August 2015.

10. Kushner, L.K., Littell, J.D. and Cassell, A.M. "Photogrammetry of a Hypersonic Inflatable Aerodynamic Decelerator in the NFAC." Proceedings from the AIAA Aerodynamic Decelerator Systems Conference. March 25-28 2013. Daytona Beach, Florida.

11. Kazemba, C. D., Cassell, A.M., Kushner, L.K., Tran, K., Quach, B.T., Li, L., Van Norman, J.W., Littell, J.D., Johnson, R.K., Hughes, S.J. and Calomino, A.M. "Determination of the Deformed Structural Shape of HIADs from Photogrammetric Wind Tunnel Data." Proceedings from the AIAA Aerodynamic Decelerator Systems Conference. March 25-28 2013. Daytona Beach, Florida.

12. Littell, J.D., Schmidt, T., Tyson, J., Oliver, S., Melis, M., Ruggeri, C. and Revilock, D. "Photogrammetry Measurements During a Tanking Test on the Space Shuttle External Tank, ET-137." Experimental and Applied Mechanics Vol. 4, pp. 111-123. 2013.

13. Stimson, C.M and Littell, J.D. "Emergency Locator Transmitter Survivability and Reliability Study." NASA TM. In Pub.

14. Littell, J.D. "Large Field Photogrammetry Techniques in Aircraft and Spacecraft Impact Testing. Proceedings from the Society of Experimental Mechanics Annual Conference. June 7-10, 2010. Indianapolis, Indiana.

15. Littell, J.D. "The Development of a Conical Composite Energy Absorber for use in the Attenuation of Crash/Impact Loads." Proceedings from the American Society for Composites Annual Conference. September 8-11 2014. San Diego, California.

16. Littell, J.D. and Stimson, C.M. "Emergency Locator Transmitter System Performance During Three Full-Scale General Aviation Crash Tests." NASA TM. In Pub.

17. Littell, J.D. and Annett, M.S. "ATD Occupant Responses from Three Full Scale General Aviation Crash Tests." NASA TM. In Pub.

REPORT DOCUMENTATION PAGE

Form Approved
OMB No. 0704-0188

1. REPORT DATE *(DD-MM-YYYY)*	2. REPORT TYPE	3. DATES COVERED *(From - To)*
01-03-2016	Technical Memorandum	

4. TITLE AND SUBTITLE

Experimental Photogrammetric Techniques used on Five Full-Scale Aircraft Crash Tests

5a. CONTRACT NUMBER

5b. GRANT NUMBER

5c. PROGRAM ELEMENT NUMBER

6. AUTHOR(S)

Littell, Justin D.

5d. PROJECT NUMBER

5e. TASK NUMBER

5f. WORK UNIT NUMBER

664817.02.07.03.02.01

7. PERFORMING ORGANIZATION NAME(S) AND ADDRESS(ES)

NASA Langley Research Center
Hampton, VA 23681-2199

8. PERFORMING ORGANIZATION REPORT NUMBER

L-20673

9. SPONSORING/MONITORING AGENCY NAME(S) AND ADDRESS(ES)

National Aeronautics and Space Administration
Washington, DC 20546-0001

10. SPONSOR/MONITOR'S ACRONYM(S)

NASA

11. SPONSOR/MONITOR'S REPORT NUMBER(S)

NASA-TM-2016-219168

12. DISTRIBUTION/AVAILABILITY STATEMENT

Unclassified - Unlimited
Subject Category 39
Availability: NASA STI Program (757) 864-9658

13. SUPPLEMENTARY NOTES

14. ABSTRACT

Between 2013 and 2015, full-scale crash tests were conducted on five aircraft at the Landing and Impact Research Facility (LandIR) at NASA Langley Research Center (LaRC). Two tests were conducted on CH-46E airframes as a part of the Transport Rotorcraft Airframe Crash Testbed (TRACT) project, and three tests were conducted on Cessna 172 aircraft as a part of the Emergency Locator Transmitter Survivability and Reliability (ELTSAR) project. Each test served to evaluate a variety of crashworthy systems including: seats, occupants, restraints, composite energy absorbing structures, and Emergency Locator Transmitters. As part of each test, the aircraft were outfitted with a variety of internal and external cameras that were focused on unique aspects of the crash event. A subset of these cameras was solely used in the acquisition of photogrammetric test data. Examples of this data range from simple two-dimensional marker tracking for the determination of aircraft impact conditions to entire full-scale airframe deformation to markerless tracking of Anthropomorphic Test Devices (ATDs, a.k.a. crash test dummies) during the crash event. This report describes and discusses the techniques used and implications resulting from the photogrammetric data acquired from each of the five tests.

15. SUBJECT TERMS

Airplane testing; Correlation; Digital image; Full scale crash testing; High-speed camera; Impact testing; Measurement techniques; Photogrammetry

16. SECURITY CLASSIFICATION OF:			17. LIMITATION OF ABSTRACT	18. NUMBER OF PAGES	19a. NAME OF RESPONSIBLE PERSON
a. REPORT	b. ABSTRACT	c. THIS PAGE			STI Help Desk (email: help@sti.nasa.gov)
					19b. TELEPHONE NUMBER *(Include area code)*
U	U	U	UU	52	(757) 864-9658